In presenting the dissertation as a partial fulfillment of the requirements for an advanced degree from the Georgia Institute of Technology, I agree that the Library of the Institute shall make it available for inspection and circulation in accordance with its regulations governing materials of this type. I agree that permission to copy from, or to publish from, this dissertation may be granted by the professor under whose direction it was written, or, in his absence, by the Dean of the Graduate Division when such copying or publication is solely for scholarly purposes and does not involve potential financial gain. It is understood that any copying from, or publication of, this dissertation which involves potential financial gain will not be allowed without written permission.

3/17/65
b

THE GEOMETRY OF STABLE BED FORMS UNDER OSCILLATORY FLOW

A THESIS

Presented to

The Faculty of the Graduate Division

by

Frank Murray Neilson

In Partial Fulfillment

of the Requirements for the Degree

Doctor of Philosophy

in the School of Civil Engineering

Georgia Institute of Technology

June, 1969

THE GEOMETRY OF STABLE BED FORMS

UNDER OSCILLATORY FLOW

Approved:

Chairman

Date approved by Chairman: April 10, 1969

ACKNOWLEDGMENTS

The writer wishes to thank all those who participated in the preparation of this thesis. Dr. M. R. Carstens, thesis advisor and Chairman of the reading committee, deserves special thanks for his encouragement and guidance during the study. The other members of the reading committee were Dr. D. V. Ho and Dr. C. S. Martin.

The writer wishes to acknowledge with sincere appreciation the financial assistance provided, through a Research Assistantship, by the Coastal Engineering Research Center, Washington, D. C., Project A-798, Engineering Experiment Station of the Georgia Institute of Technology.

TABLE OF CONTENTS

TABLE OF CONTENTS (Continued)

LIST OF TABLES

LIST OF ILLUSTRATIONS

LIST OF ILLUSTRATIONS (Continued)

NOMENCLATURE

Symbol	Quantity	Dimensions (F-L-T)
a	water-motion amplitude	L
A	coefficient (Appendix A)	L
C	coefficient	none
C_D'	coefficient of drag of a sediment particle in quiescent fluid	none
D_g	median diameter of bed-material particles	L
$f(\ )$	function of	none
f_1, f_2, f_3	functional expressions	none
g	acceleration due to gravity	LT^{-2}
i, j	summation variables	none
N_s	sediment number ($N_s \equiv \frac{u}{\sqrt{(s-1)gD_g}}$)	none
N_{sc}	sediment number at incipient motion	none
N_{scd}	sediment number at which ripples will not propagate	none
N_{sm}	sediment number based on maximum, mainstream, fluid velocity ($N_{sm} \equiv \frac{U_m}{\sqrt{(s-1)gD_g}}$)	none
q_s	volumetric rate of transport of bed material per unit width of bed	L^2T^{-1}

NOMENCLATURE (Continued)

Symbols	Quantity	Dimensions
q_{sm}	maximum volumetric rate of transport of bed material	L^2T^{-1}
s	ratio of specific weight of a sediment particle to the specific weight of water -- $s = \gamma_s/\gamma$	none
t	time	T
Δt	incremental time	T
T	water-motion period	T
u	local fluid velocity at particle level	LT^{-1}
u_c	threshold (incipient) local fluid velocity at particle level	LT^{-1}
u_e	bed-material pickup velocity	LT^{-1}
U	mainstream velocity	LT^{-1}
U_m	maximum mainstream velocity	LT^{-1}
V	volume, per unit width of bed, of material removed from the upstream face	L^2
V_e	volume, per unit width of bed, of material eroded from the upstream face	L^2
V_f	volume, per unit width of bed, of bed material deposited along the upstream face	L^2
x	horizontal distance measured from the dune trough	L
Δx	incremental horizontal distance	L
y	elevation above the dune trough	L
Δy	incremental vertical distance	L

NOMENCLATURE (Continued)

Symbol	Quantity	Dimensions
β	limit of a summation	none
γ	specific weight of fluid	$F\ L^{-3}$
γ_s	specific weight of sediment particles	$F\ L^{-3}$
$\Delta\gamma$	bouyant specific weight -- $\Delta\gamma = \gamma_s - \gamma$	$F\ L^{-3}$
Γ	limit of a summation	none
δ	net forward movement of the upstream face	L
δ_e	forward movement, due to erosion, of the upstream face	L
δ_f	backward movement, due to deposition, of the dune face	L
ζ	limit of a summation	none
η	dune height -- trough-to-crest	L
θ	inclination of the bed surface	none
λ	dune wave length -- crest-to-crest	L
λ_s	wave length of a stable dune	L
μ	dynamic viscosity of fluid	$F\ L^{-2}\ T$
ρ	mass density of fluid	$F\ L^{-4}\ T^2$
ρ_s	mass density of sediment particles	$F\ L^{-4}\ T^2$
σ	geometric standard deviation of particle diameter	none
τ	lag-time between time of maximum rate of sediment transport and time of maximum water motion velocity	T

NOMENCLATURE (Continued)

Symbol	Quantity	Dimension
Φ	angle of repose of the bed material	none

Subscripts Denoting Locations in the x-t Plane

Symbol	Significance	Figure(s)
a	denotes the location in space and time corresponding to the least value of x at which erosion occurs	7, 10, 13
b	denotes the location corresponding to the least value of x at which deposition occurs along the upstream face during one-half cycle	7
c	denotes the crest	7, 13
c1	denotes the location, in space and time, at which erosion first occurs on the upstream face	7, 10
c2	denotes the location, in space and time, at which erosion ceases on the upstream face	7, 10
d	denotes the toe of the fill on the downstream face of the crest near the end of the half-cycle	10
n	denotes the initial point on the particle path $\overline{nn}$	13
q	denotes the initial point on the particle path $\overline{qq}$	12
r	denotes a general location on the upstream face	10, 11, 12, 13
r1	denotes the time at which erosion first occurs at location r.	10, 11, 12
r2	denotes the time at which erosion ceases at location r.	10, 11, 12

SUMMARY

The subject of this study is the dunes which develop as fluid is made to oscillate, with simple-harmonic motion, across an erodible bed. The object is to describe the geometrical characteristics of bed forms in terms of fluid and sediment properties, and the fluid-motion characteristics. Dunes created by the oscillation of water over natural beach sands are of particular practical interest.

The model used to classify bed forms is a plane sediment bed subjected to oscillatory fluid motion. In this model the plane bed may remain plane or it may become deformed. If the bed remains plane the surface particles may be immobile (lower velocities) or mobile (higher velocities). In the range between the immobile plane-bed velocities and the mobile plane-bed velocities the bed-surface will either deform spontaneously or may be induced to deform by means of a disturbance in the flow near the bed. The irregularities which first appear on the bed are transient features termed ripples. Subsequent to the appearance of ripples larger features, dunes, develop on the bed. The dunes enlarge until they reach an equilibrium size.

The development of a duned bed is analyzed by evaluating erosion and deposition along the bed during each one-half cycle of water motion. The theoretical development is summarized as follows.

Experimental evidence indicates that, for a range of water motion velocities, dunes are two-dimensional. The profiles of these dunes are similar -- the ratio of

dune height to dune wave length being about 0.18. Since the flow along the upstream face of the dune accelerates in the direction of the crest the local fluid velocity, u, at particle level is given by a solution for irrotational flow. Since separation occurs at the crest and a vortex occurs in the lee of the crest the velocity distribution along the downstream face is not readily obtainable. The velocity distribution along the upstream face was obtained by flow-net analysis using a typical two-dimensional dune profile. The separation line was assumed to be a circular arc which was tangential to the dune crest and passed through the center of the dune trough. The velocity distribution along the upstream face is

$$\frac{u}{U_m} = 2.4 \ \frac{x}{\lambda} \cos \left(\frac{2\pi t}{T} \right)$$

in which U_m is the maximum mainstream velocity, λ is the dune wave length (crest-to-crest) and T is the water motion period. The distance x is measured from the center of the trough of the dune and time, t, is from t equal -T/4 at the start of one-half cycle of water motion.

If the velocity, u, is less than a threshold velocity, u_c, sediment grains will not move. Whenever and wherever $u > u_c$ sediment grains are removed from the bed. The following empirical expression was used to evaluate the volumetric rate of removal of the bed material.

$$\frac{u_e}{u} = 10^{-4} N_s^4 \left[1 - \left(\frac{u_c}{u} \right)^2 \right]^{10}$$

in which u_c is the pickup velocity -- the volume transport velocity which describes the rate at which the bed surface recedes, normal to the bed surface, as sediment grains are scoured from the bed; and N_s is the local sediment number -- $N_s \equiv u/\sqrt{(\gamma_s/\gamma - 1)gD_g}$ in which γ_s is the unit weight of the sediment particles, γ is the unit weight of the fluid, g is the acceleration due to gravity, and D_g is the mean diameter of the sediment particles. A sediment particle, which is scoured from the bed, is assumed to be transported at the local fluid velocity, u. In addition, sediment particles are assumed to deposit along the upstream face whenever and wherever the local fluid velocity, u, has decelerated to the threshold velocity u_c. Particles eroded from, but not deposited on, the upstream face are swept over the crest and deposited in the lee of the crest.

The theory allows the evaluation of the following quantities: (a) the total volume eroded from, the net volume deposited on, and the net volume removed from the upstream face of a dune during one-half cycle of water motion; (b) the displacement and shape of the upstream face of a dune; and (c) the volume rate of transport of material at any time, during the half-cycle, and location, along the upstream face. These quantities (a, b, and c above) are functions of the bed-material and fluid properties, the water-motion characteristics, and the size and shape of the bed forms. The manner in which the sediment grains are deposited along the lee face of a crest is not described by the theory.

Occurrences on a plane bed subjected to oscillatory water motion are described in terms of the theoretically evaluated quantities mentioned above. In particular the following occurrences are considered.

A. Transient Conditions

Since dunes evolve from an initially rippled bed, it is necessary to know the size and type of ripple occurring on the bed in order to describe the development, from the inception of a dune to the existence of stable dunes, of a duned bed. Precise information regarding the size of ripples are not available. Experimental data, concerning the delineation of the conditions causing either a mobile plane-bed, a spontaneously rippled-bed, an induced rippled-bed, or an immobile plane-bed to exist, are available. These four regions are delineated in terms of the pertinent variables subsequently used to describe the development of the duned bed.

B. Development of a Duned Bed From a Plane Bed

Inasmuch as the shape of the downstream face of a growing crest is unknown the analysis does not permit the evaluation of the rate of development or the time required for the dunes to grow to equilibrium. However the analysis does indicate that:

(a) For a constant value of the critical sediment number, N_{sc}, and the parameter u_c/U_m, the volume, V_e, eroded from the upstream face of a dune during one-half cycle of water motion is essentially independent of the size of the dune,

(b) For a particular bed material the volume, V_e, is greater at lower values of u_c/U_m -- consequently the time of development is less at lower values of u_c/U_m,

(c) For a particular value of u_c/U_m the volume, V_e, is greater for higher

values of N_{sc} -- consequently the time of development is less for higher values of N_{sc}.

C. Types of Stable Dunes

Two-dimensional, three-dimensional, and transitional dunes are delineated in terms of the parameters, $a N_{sc}^4/\lambda$ and u_c/U_m, and the variable θ -- θ is the slope of the upstream face at the beginning of the half cycle and a is the water motion amplitude.

D. Wave Length of Stable Dunes

The wave length, λ_s, of a stable two-dimensional dune is obtained from

$$\frac{a}{\lambda_s} \approx 0.8 - \frac{2u_c}{3U_m}$$

This relationship is based on the assumption that the extension of the area of fill on the downstream face is proportional to the water motion amplitude. This assumption is a logical consequence of the fact that for higher values of u_c/U_m the movement of the crest is small.

CHAPTER I

INTRODUCTION

A. Definition of the Problem

The water motion near the sea bed, during the passage of a series of first-order Stokian waves, is simple harmonic and parallel to the bed. The subject of this study is the dunes which develop on an erodible bed as water is made to oscillate, with simple-harmonic motion, across the bed. The object is to determine functional relationships between the geometrical parameters, which describe the bed forms, and the parameters which describe the flow characteristics and the bed-material properties.

Knowledge of the size and shape of bed forms under oscillatory fluid flow is of particular practical value to the coastal engineer. Energy dissipation in the flow over an erodible bed and bed-load sediment transport along an erodible bed are obviously affected by the shape of the sediment-fluid interface. In addition, the techniques presented in the theory provide a new approach to any problem involving localized scour and deposition. For example, problems concerning localized scour around obstacles located on the bed could be approached by a similar analysis.

Data on bed forms are available from controlled experimental investigations and from measurements on the ocean floor. The experimental techniques employed in laboratory investigations have been of three types. Data have been obtained by

oscillating a sediment bed through still water, by using surface waves to generate oscillatory water motion near an erodible bed, and by producing simple-harmonic water motion over a stationary, erodible bed.

A convenient model for observing the nature of bed forms under oscillatory flow is a plane erodible-bed subjected to oscillatory water motion. The plane bed becomes deformed and, in time, attains a stable or equilibrium configuration. According to Carstens and Neilson (1), who used this technique, the first features to appear on the bed are short in wave length and consist of bands of sediment grains rolling back and forth along the interface. Subsequently larger features, characterized by active vortices, develop on the bed. These vortex features enlarge and, in time, become stable bed forms. For a range of maximum fluid-motion velocities, vortex features are two-dimensional and amenable to analysis. These two-dimensional vortex features are the bed forms for which the theory developed herein is intended to apply.

B. Terminology

The terminology used to describe bed features under oscillatory flow is not uniformly established. The terminology adhered to in this study, and a description of the phenomena which occur during the development of the bed, is outlined in the following discussion. The terminology is consistent with that of Bagnold (2), Carstens and Neilson (1), and Carstens, Neilson, and Altinbilek (3).

A plane erodible bed does not always become deformed under oscillatory flow. For extremely low values of maximum water-motion velocity and also for

extremely high values of maximum water-motion velocity a plane interface will remain plane. In the former situation, the sediment particles at the interface are stationary and therefore, the initially plane bed is not changed by the water motion. In the latter situation, sediment particles in the upper region of the bed are swept back and forth during a cycle . The surface of the bed, which remains plane, resembles a dense fluid undergoing oscillatory motion. For water-motion velocities between these two plane-bed conditions, the bed surface either will become deformed or, for lower velocities, can be induced to become deformed.

One general classification of bed forms considers the manner in which sediment particles move along the interface. A rolling-grain feature is termed a ripple whereas a vortex feature is termed a dune. In other words, a ripple is a low-amplitude bed-form typified by bands of sediment particles rolling on the surface of the bed whereas a dune is a larger bed form typified by vortex action in the lee of the crest. Ripples are a transient bed-form which are replaced by dunes as the water-motion continues.

Ripples are reported (1) to be of two types. Above a particular water-motion velocity uniform bands of rolling sediment-grains occur simultaneously all over the bed. These ripples are termed spontaneous ripples. For lower water-motion velocities, rolling sediment-grains occur adjacent to a disturbance placed in the flow near the bed. These ripples are termed induced ripples.

Dunes exist throughout a range in maximum water-motion velocities. Three types of dunes, typified by the geometry of the bed forms, are reported in the literature. Extensive data (1, 2, 3, 4, 5, 6, 7) are available on two types, namely,

two-dimensional and three-dimensional dunes. Three-dimensional dunes exist over a range of maximum water-motion velocities which extends up to the mobile plane-bed condition. These dunes are irregular in both plan and profile. That is, the dune crests and troughs are broken and the elevations of the crests, and the troughs, vary from dune to dune. Figure 1 is a topographic map (3) of a three-dimensionally duned bed. Two-dimensional dunes exist over a range of maximum water-motion velocities which extend down to the immobile plane-bed condition. The profiles of these dunes are the same for each dune on the bed and, in plan, the crests are straight, parallel, and unbroken. The crests are alined transverse to the direction of the water motion. Figure 2 is a topographic map (3) of a two-dimensionally duned bed. The demarcation between two- and three-dimensional dunes is not clearly defined. In fact, there appears to be a range of maximum water-motion velocities within which the bed may be two-dimensional in some areas and three-dimensional in other areas.

The third type of dune observed in laboratory investigations (2, 8) are termed brick-pattern dunes. These dunes form a regular, three-dimensional pattern over the bed. The crests are alined normal to the direction of water motion similar to the crests of two-dimensional dunes. However the crests are intersected by short, transverse ridges which terminate, and break joint, at each crest. These features have been observed when the ratio of water-motion amplitude to dune wave length is small.

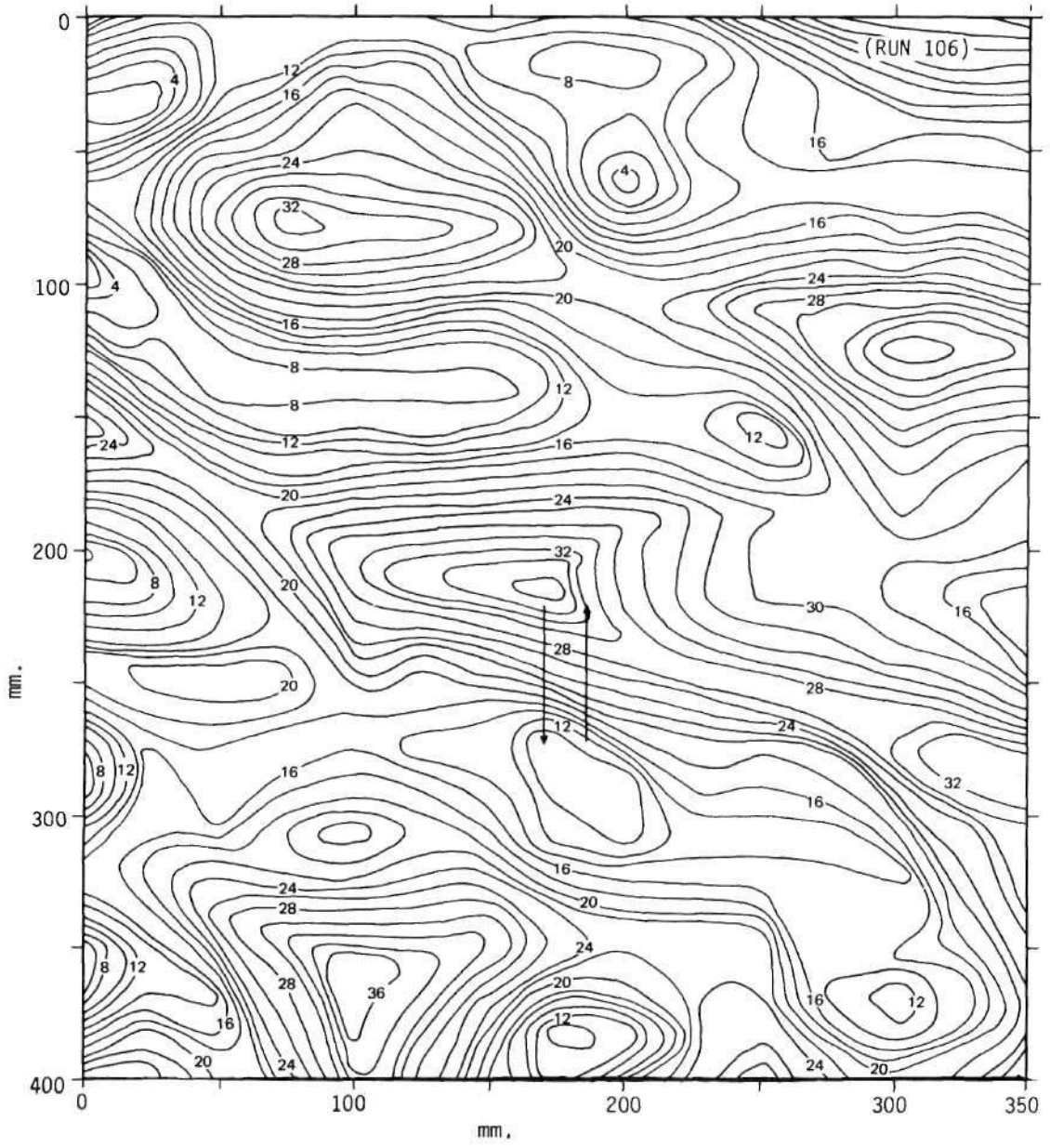

Figure 1. Topographic Map of Three-Dimensional Dunes (3).

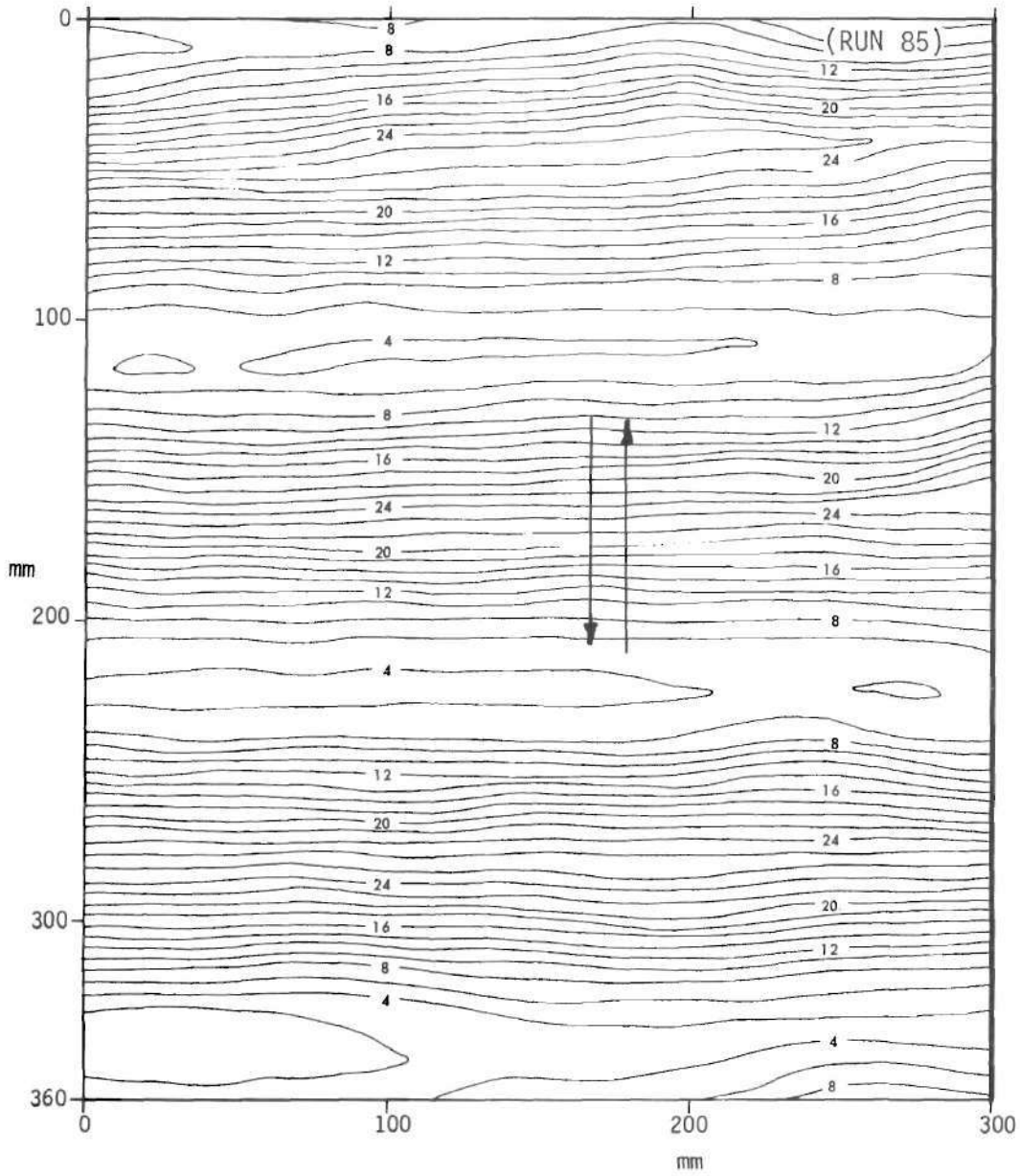

Figure 2. Topographic Map of Two-Dimensional Dunes (3).

C. Survey of the Literature

An extensive review of the literature is available in a recent (1966) report by Kennedy and Falcon (4). Since the review is complete and up-to-date, the reader is referred to the report (4) for the chronological development of literature pertaining to bed forms under oscillatory flow.

The most extensive observations of bed forms as they occur in nature has been presented by Inman (7). Ripples and dunes were observed on the sea-bed. These data are important inasmuch as they reveal the complex interplay between the ocean surface waves, the water-motion velocities near the bed, the properties of the bed material, and the characteristics of the sediment-water interface. Three difficulties in analyzing this data are apparent. Firstly, the pertinent variables are uncontrolled -- the water-motion characteristics and the properties of the bed material are those occurring naturally at the time and location of the observations. Secondly, water-motion characteristics near the bed are difficult to measure -- in most cases water-motion characteristics near the bed were computed from measurements of the surface-wave profiles. Thirdly, inasmuch as the development of a duned bed is a time-dependent phenomena, the question arises as to what stage of development exists on the bed; that is, are the bed forms enlarging, decaying, or stable at the time of observation.

Laboratory investigations of bed forms under oscillatory flow have been performed using three different types of apparatus. A versatile technique has been to oscillate a bed of sediment within a container of quiescent fluid. This technique was used by Bagnold (2) and by Manohar (8). Bagnold allowed a tray,

in the form of a circular arc, to pendulate through still water. The sediment bed was placed on the tray. Manohar used a trolley which oscillated horizontally through still water. The sediment bed was located on the trolley. Some objections to using an oscillating sediment bed in quiescent water to simulate a stationary sediment bed under oscillatory water-motion have been suggested (4, 9). In particular, the acceleration of fluid particles and the pressure fluctuations in the immediate vicinity of the bed, and the turbulence configuration are not reproduced. Secondary disturbances, caused by any moving body in an otherwise quiescent fluid, may also affect the conditions near the bed. Consequently the motion of a sediment particle relative to the bed may be different in the case of an oscillating bed than in the case of an oscillatory water-motion. Another technique (4, 5, 6) is to observe bed forms occurring on the floor of wave channels. Surface waves of short periods and relatively large amplitudes are used to create oscillatory water-motion characteristics. However, the water-motion characteristics near the bed are necessarily limited to a narrow range and, in addition, are difficult to measure. The third technique (1, 3) is to observe bed forms on the floor of an oscillatory-flow water-tunnel. The water-motion characteristics* and the bed-material properties are the controlled variables and these are varied over a large range in values. An obvious advantage of this method is the positive control of the independent variables, that is, the water-motion characteristics and the bed-material properties.

- - - - - - -

*The available data (2, 3) pertaining to the geometry of bed forms in an oscillatory-flow water-tunnel are from experiments in which the amplitude of water-motion is varied and the period is kept approximately constant. Therefore, the controlled water-motion variable is the amplitude of the oscillations.

D. Summary of Available Data

Various procedures have been used to obtain information pertaining to the deformation of a sediment-water interface under oscillatory flow. Since the observed configuration of the sediment bed may be significantly affected by the initial conditions of the experiment, the methods used by each investigator are an important part of his data. Therefore a brief description of the apparatus, bed materials, and procedures used by each investigator is included in this section. A brief analysis of the parametrical dimensionless variables is also included.

1. Techniques of Quoted Authors

Bagnold (2) observed the characteristics of the sediment-water interface of an erodible bed oscillating through still water. His apparatus consisted of a cradle, in the shape of an arc, on which the sediment bed was placed. The cradle was suspended from a pivot and was made to pendulate through still water. The period and the amplitude of the oscillation were the controlled water-motion variables. The speed of oscillation ranged from the minimum value for development of bed forms to a maximum value at which the mass of sediment would slide along the floor of the cradle. Eight types of bed materials were used in the tests; these being two sizes of coal sediments, four sizes of quartz sands, and two sizes of steel particles. The median diameter of the particles ranged from 0.09 mm to 2.50 mm. The characteristics of the water motion in the vicinity of the bed were observed and the geometrical characteristics of the bed forms were measured.

Carstens, Neilson, and Altinbilek (3) investigated the characteristics of the sediment-water interface of an erodible bed immersed in an oscillatory-flow

water tunnel. The amplitude of the oscillatory water-motion was a controlled variable whereas the period of the oscillations maintained a constant value of about 3.6 seconds. The amplitude of oscillation ranged from a value below that required for development of bed forms to a maximum value of about 1.5 ft. Three types of bed materials, corresponding to fine, medium and coarse sands, were used. Many phenomena associated with oscillatory water-motion over a sediment bed were investigated. As examples, an incipient-motion criteria was developed and data regarding the geometrical properties of bed forms, the development of the bed, and the energy-dissipation in the flow over the bed were taken.

Kennedy and Falcon (4) investigated the stability of an erodible bed under water waves and obtained experimental information regarding the geometry of the bed forms. The experiments were performed in a glass-walled channel which was 100-ft. long, 2.5-ft. wide, and 3-ft. deep. The water waves ranged in period from 0.26 seconds to 3.16 seconds or from 0.6 seconds to 12 seconds depending on the type of wave generator used. The corresponding maximum wave heights were 0.5 ft. and 1.0 ft. The maximum water-motion velocity and the water-motion amplitude in the vicinity of the bed were computed from surface wave profiles. The sediment bed, which was 2.75-inches thick, was placed along a 10-ft. reach of the channel. Two sizes of quartz sands and two sizes of plastic sediments were used in the experiments. A moveable point gage was used to measure the height and length of the bed forms.

Yalin and Russell (5) performed two series of experiments in a wave channel. The purpose of the experiments was to investigate a similarity criteria which

relates the geometry of bed forms and the sediment transport rate in a model situation to the corresponding measurements in a prototype situation. The period of the water waves was 1.0 second in one series of tests and 1.82 seconds in the other. For each series, the water-wave height was the controlled water-motion variable. The orbital lengths in the vicinity of the bed were observed, during the calibration phase, by means of a pendulum arrangement which oscillated with the water motion. During the experiments the wave heights were measured and, by means of the calibration data, the orbital lengths were computed. The sediment bed was 26.2-ft. long, 2.46-ft. wide, and at least 1.18-inches deep. The bed material was coal particles in the "model" series of tests and perspex pellets in the "prototype" series. The heights and lengths of the bed forms were averaged over a system of dunes.

Inman and Bowen (6) performed two series of experiments to determine the quantity of sand transported along the bed under the action of surface waves. The experiments were performed in a wave channel 94-ft. long in which the average water depth was 3.94 inches. The period of the water waves was 1.4 seconds in one series of tests and 2.0 seconds in the other. For each series the wave height was the controlled water-motion variable with a maximum value of 5.91 inches. A steady current of 0.788 inch/sec, 1.576 inch/sec, and 2.364 inch/sec was introduced from the down-wave end of the channel to add drift current to the oscillatory flow velocity. The sediment bed was 36.1-ft. long and 2.0-ft. wide. The bed material was a quartz sand for all the tests.

Inman (7) observed the geometrical properties of bed forms existing on

the ocean floor during storm periods. The observations were made in situ in the nearshore area off La Jolla, California. Divers measured, and made photographs of, the ripples while water-wave characteristics were observed, simultaneously, on the surface. The Airy theory for waves of small amplitude was used, in regions of deeper water, to compute the water-motion characteristics near the bed. Whereas the solitary-wave theory was used for similar computations near the breaker zone. The measurements were taken in depths ranging upwards to 120 ft. Bed forms were observed, but not measured, at a depth of 170 ft. The bed material ranged, in median diameter, from about 0.1 mm to 0.6 mm.

Manohar (8) observed the characteristics of the sediment-water interface of an erodible bed oscillating in still water. A trolley, on which the sediment bed was located, was oscillated in a horizontal plane within a glass-walled, water-filled flume. Many observations of the occurrences at the interface were made during this extensive testing program. The tests concerning the geometry of bed forms were conducted as follows. The tray-motion amplitude was held constant while the period was decreased in increments for each test. The maximum velocity of oscillation ranged from the immobile, plane-bed range to the mobile plane-bed range. For each experiment, that is for each speed, the run was continued until the bed attained a stable configuration. Four types of bed-materials were used in the experiments concerned with the geometry of bed forms -- two sizes of quartz sands and two sizes of plastic pellets. The sediment bed was 6.5-ft. long by 11.5-inches wide.

2. Dimensionless Parameters

As of this date no satisfactory theory is available with which to predict the stable bed configuration as a function of the water-motion characteristics and the fluid and bed-material properties. Considerable experimental and field measurements of the configurations of the bed are available. Some of these data are assembled and tabulated in Appendix B. A discussion of the variables, and the dimensionless combinations of the variables, will be undertaken in order to explain the manner of presentation of the data.

The dependent variables describing the geometry of dunes are the trough-to-crest height, η, and the wave length, λ. The fluid-property variables are the fluid density, ρ, and the fluid specific weight, γ. The fluid viscosity is omitted as a variable by virtue of the negligible boundary layer thickness anticipated in the flow over the dunes. The fluid specific weight is a pertinent variable inasmuch as the stabilizing force on a bed particle is a function of the submerged weight; that is, since the submerged weight of a particle is proportional to $\gamma_s - \gamma$, or $\Delta\gamma$, the specific weight of the sediment, γ_s, and the fluid, γ, are both pertinent variables. The sediment-property variables are mean diameter, D_g, geometric standard deviation with respect to size, σ, specific weight of the sediment, γ_s, and the particle shape. The omission of the sediment density, ρ_s, is based on the assumption that the inertial reaction of the sediment particles is small compared to the lift and drag forces on the particle. The fluid-flow variables are any two of the following three variables: the maximum water-motion velocity, U_m, in the vicinity of the bed, the water-motion amplitude, a, in the vicinity of the bed, and the period, T,

of the water motion. Since the two specific weights are involved in a known way, that is by submerged weight, they can be replaced by the single variable $\Delta\gamma$. Therefore one can expect

$$\eta \text{ or } \lambda = f(U_m, T, \rho, \Delta\gamma, D_g, \sigma_g \text{ particle shape}) \tag{1a}$$

or

$$\eta \text{ or } \lambda = f(U_m, a, \rho, \Delta\gamma, D_g, \sigma_g, \text{ particle shape}) \tag{1b}$$

or

$$\eta \text{ or } \lambda = f(a, T, \rho, \Delta\gamma, D_g, \sigma_g, \text{ particle shape}) \tag{1c}$$

Two parameters, σ_g and particle shape, are dimensionless. The remaining independent variables may be combined into any two of the following three dimensionless parameters depending on which of the three functional relationships is considered.

$$\pi_1 = T\sqrt{\frac{(s-1)g}{D_g}} \quad ;$$

$$\pi_2 = \frac{U_m}{\sqrt{(s-1)_g D_g}} \quad ;$$

and

$$\pi_3 = \frac{a}{D_g}$$

Since any pertinent length dimension may be used to non-dimensionalize the dune-geometry characteristics, or dependent variables, any of the following combinations may be of interest.

$\pi_4 = \eta/D_g$; $\pi_5 = \lambda/D_g$; $\pi_6 = \eta/a$;

$\pi_7 = \lambda/a$; and $\pi_8 = \eta/\lambda$.

The available data pertaining to the geometry of dunes are tabulated, Appendix B, using the dimensionless combinations π_1, π_2, π_3, π_6, π_7, and π_8. The values of particle diameter, water-motion period, and sediment-particle specific gravity are also listed in Appendix B.

E. Theory

In order to achieve an understanding of the pehnomena occurring at the interface of the sediment bed and the oscillating water, a simplified theory is presented. Basically the theory evaluates the localized scouring process along the upstream face of a two-dimensional dune. The concept is that the upstream face of the dune is the area in which scour occurs and that the downstream face is simply a dumping area for sand grains carried over the crest. Consequently, a face of a crest is a region of scour during one half-cycle of water motion and a region of fill during the following half-cycle. An equilibrium condition exists when the volume and region of scour occurring during one half-cycle is identical to the volume and region, respectively, of fill during the following half-cycle.

CHAPTER II

THEORY

A. Profile of a Two-Dimensional Dune

The experimental observations (3) which pertain to two-dimensional dunes indicate that the profiles of these dunes are similar. The value of the ratio of height to wave length for two-dimensional dunes is shown to be between 0.15 and 0.20 and to be independent of the maximum water-motion velocity, the size of the sediment particles, and the specific gravity of the particles. Inasmuch as these experiments (3) were performed with coarse, medium, and fine sands and covered the complete range of maximum water-motion velocities, within which two-dimensional dunes exist for each of these bed materials, the profile obtained in these tests is used herein as the typical two-dimensional dune profile. The measured profile of the dunes is shown in Figure 3.

B. Velocity Distribution

Flow over a dune under oscillatory flow is illustrated by the motion picture frames (3) presented in Figure 4. The flow separates from the bed at the dune crest and a vortex forms in the lee of the crest. The flow reattaches to the bed in the trough. The velocity at a protruded-particle height is zero in the trough and increases continuously along the upstream face of the crest to attain a maximum value at the crest. Sand grains experiencing bed-load movement are carried along

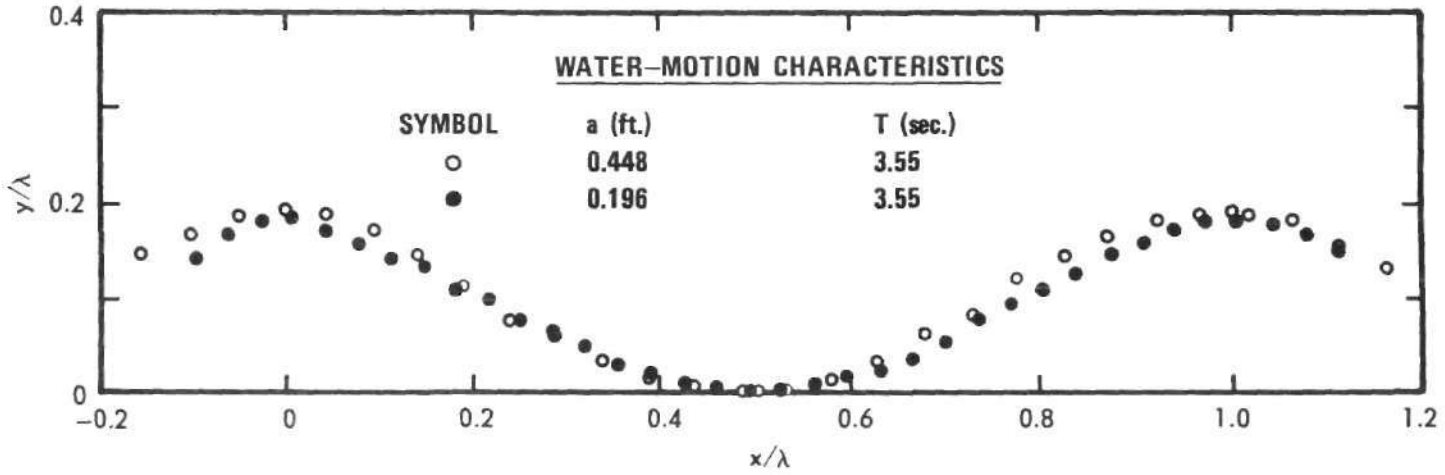

Figure 3. Profile of Two-Dimensional Dunes (3) (Medium Sand; s = 2.47, D_g = 0.297 mm).

(a) t/T = -0.25

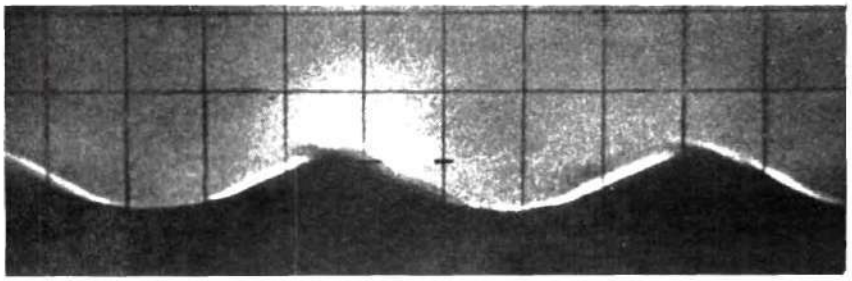

(b) t/T = -0.14

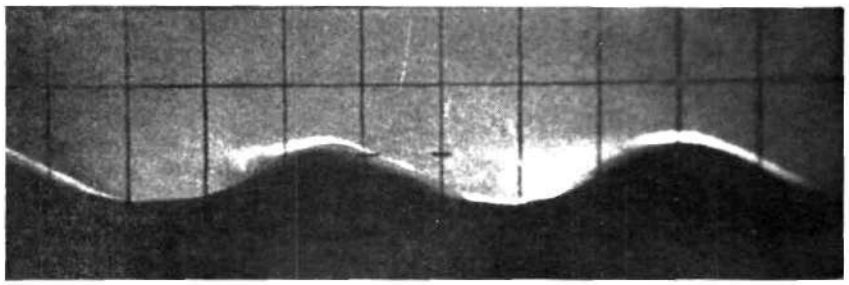

(c) t/T = -0.01

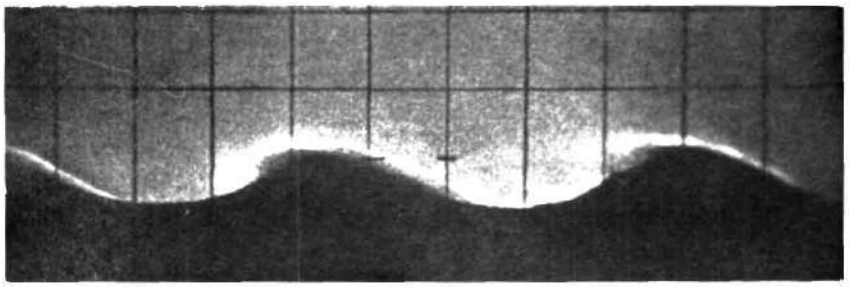

(d) t/T = 0.12

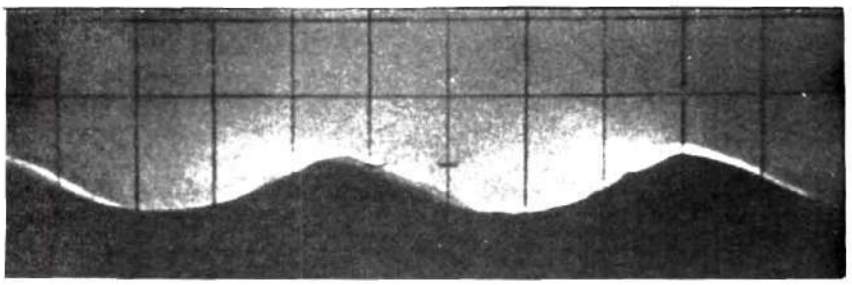

(e) t/T = 0.25

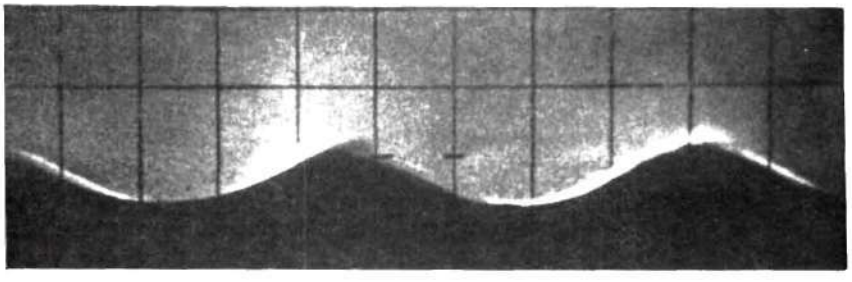

Figure 4. Flow Over Two-Dimensional Dunes.

the upstream face of the crest and are dumped into the vortex in the lee of the crest. This flow pattern persists during the major portion of one-half cycle. Towards the end of the half-cycle the lee-vortex is ejected into the mainstream flow. During the following half-cycle the flow pattern is repeated, except that the previous upstream face of the crest is now the lee face.

The boundary-layer thickness, along the upstream face of a dune, may be assumed to be negligible. Firstly, since the boundary layer of an oscillatory flow is reformed and must develop during one half-cycle, the time for the development of the boundary layer is small and precludes the development of a thick boundary layer. Secondly, the pattern of separation at the crest, reattachment in the trough, and converging flow along the upstream face are flow conditions under which boundary-layer development is suppressed even under steady-flow conditions. Since the boundary-layer thickness is assumed to be negligible, the distribution of the velocity, u, along the upstream face can be determined from a solution for irrotational flow.* The measured profile of the two-dimensional dunes, previously shown in Figure 3, was approximated for the irrotational flow solution as shown in Figure 5(a). The velocity distribution along the upstream face of the crest is shown in Figure 5(b). As shown in Figure 5(b) a reasonable approximation for the velocity distribution is

$$u = \frac{2.4xU}{\lambda} \tag{2}$$

in which x is distance measured from the center of the trough and U is the mainstream velocity some distance above the bed. The mainstream velocity, U,

- - - - -

*Refer to Appendix C, page 97.

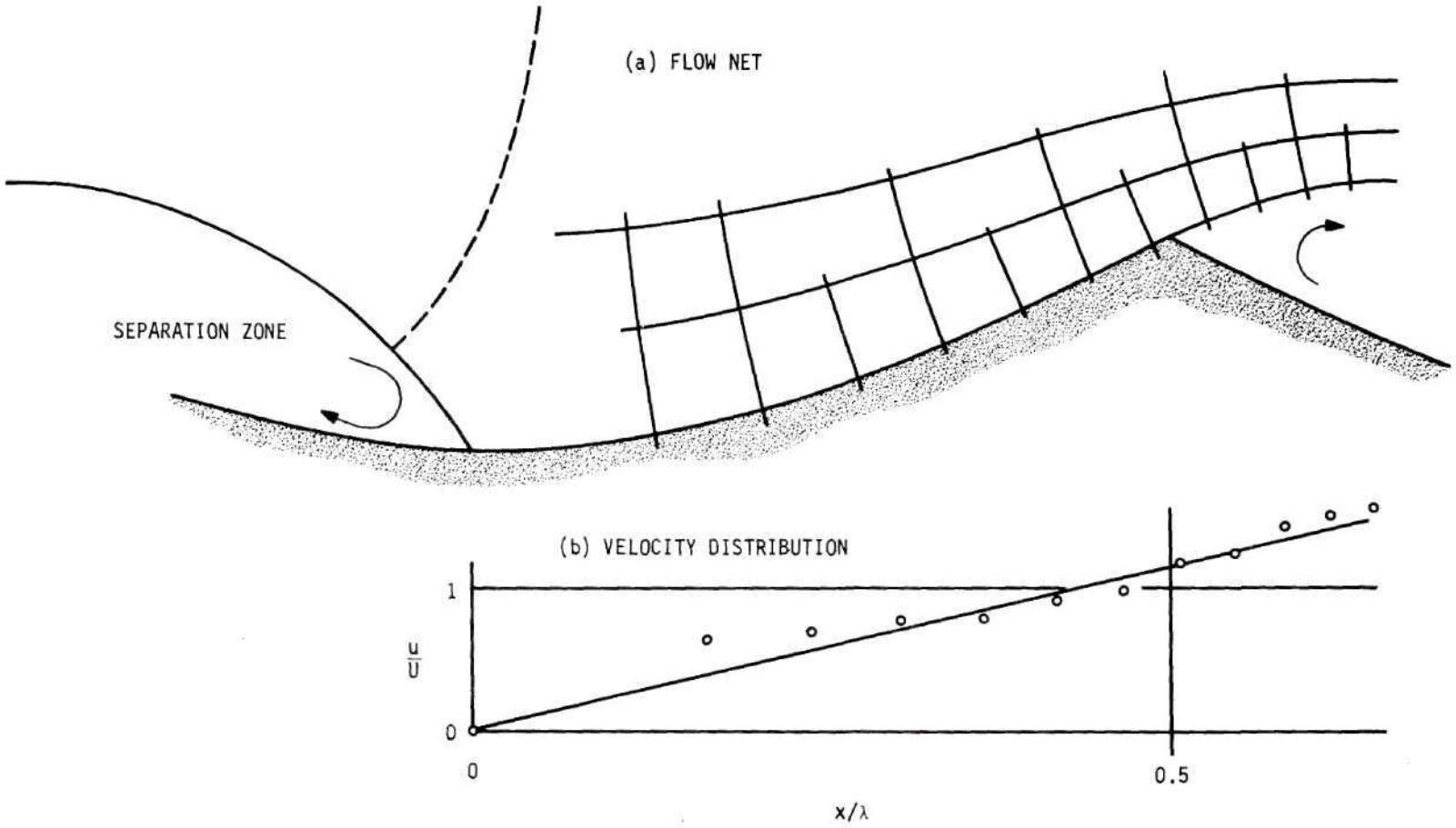

Figure 5. Velocity Distribution Along the Upstream Face (3).

is simple harmonic and parallel to the bed the space-time variation in velocity, u, along the upstream face of the crest may be expressed by

$$\frac{u}{U_m} = 2.4 \left(\frac{x}{\lambda}\right) \cos\left(2\pi \frac{t}{T}\right) \tag{3}$$

C. Incipient Motion

Whenever and wherever the velocity, u, is greater than an incipient or threshold velocity, u_c, sand grains will move with the flow. Using equation 3 to describe the velocity, an incipient motion condition exists when

$$\frac{u_c}{U_m} = 2.4 \left(\frac{x}{\lambda}\right) \cos\left(2\pi \frac{t}{T}\right) \tag{4}$$

along the upstream face of the dune; that is, during the time interval from -T/4 to T/4 and extending from the trough where x equals zero to the crest where x equals $\lambda/2$.*

Carstens (3) has formulated the following incipient-motion criterion,

$$\frac{u_c^2}{(s-1) g D} = \left(\frac{\tan \Phi \cos \theta + \sin \theta}{1 + \tan \Phi} \right) \frac{8.2}{C_D'} \tag{5}$$

in which, Φ is the angle of repose of the sediment, θ is the angle of inclination of

- - - - - - -

*During the following time interval, which is from T/4 to 3T/4, the flow reverses with the result that this bed area becomes a downstream face where only deposition occurs.

the bed, and C_D' is the coefficient of drag of a sediment particle in an infinite, quiescent fluid. Ignoring the bed slope, θ, or simply letting θ be zero, u_c is seen to be a function of C_D', D_g, s, and Φ in equation 5. In other words, the critical velocity, u_c, is a function of the bed-material and fluid properties. Thus for a given oscillatory flow over a given bed material, the ratio u_c/U_m, shown in equation 3, has a constant value.

The regions and times of "movement" and "no movement" for a particular bed material and given oscillatory motion are delineated by means of equations 4 and 5. Figure 6 is a schematic space-time diagram illustrating these regions for one dune. The crest position is, of course, midway between two adjacent troughs. At a constant value of x, which is described by a horizontal line in Figure 6, the alternations between upstream face and downstream face are noted at -3T/4, -T/4, T/4, and 3T/4. The upstream face is divided into regions and times of movement and no movement. The cross-hatched region on the downstream face is merely an extension of the time during which bed material is carried over the crest to be deposited on the downstream face. Even though the cross-hatching extends from crest to trough, the major portion of the deposition occurs close to the crest.

D. Particle Paths

Assuming that any sediment particle which moves is transported at the same velocity as the water, then equation 3 expresses the velocity of the particle along the upstream face of the crest. The motion is initiated when the bottom velocity, u, is equal to the threshold velocity, u_c. In addition, the sand-grain motion is presumed to cease when and where u decreases to u_c. Hence, the regions

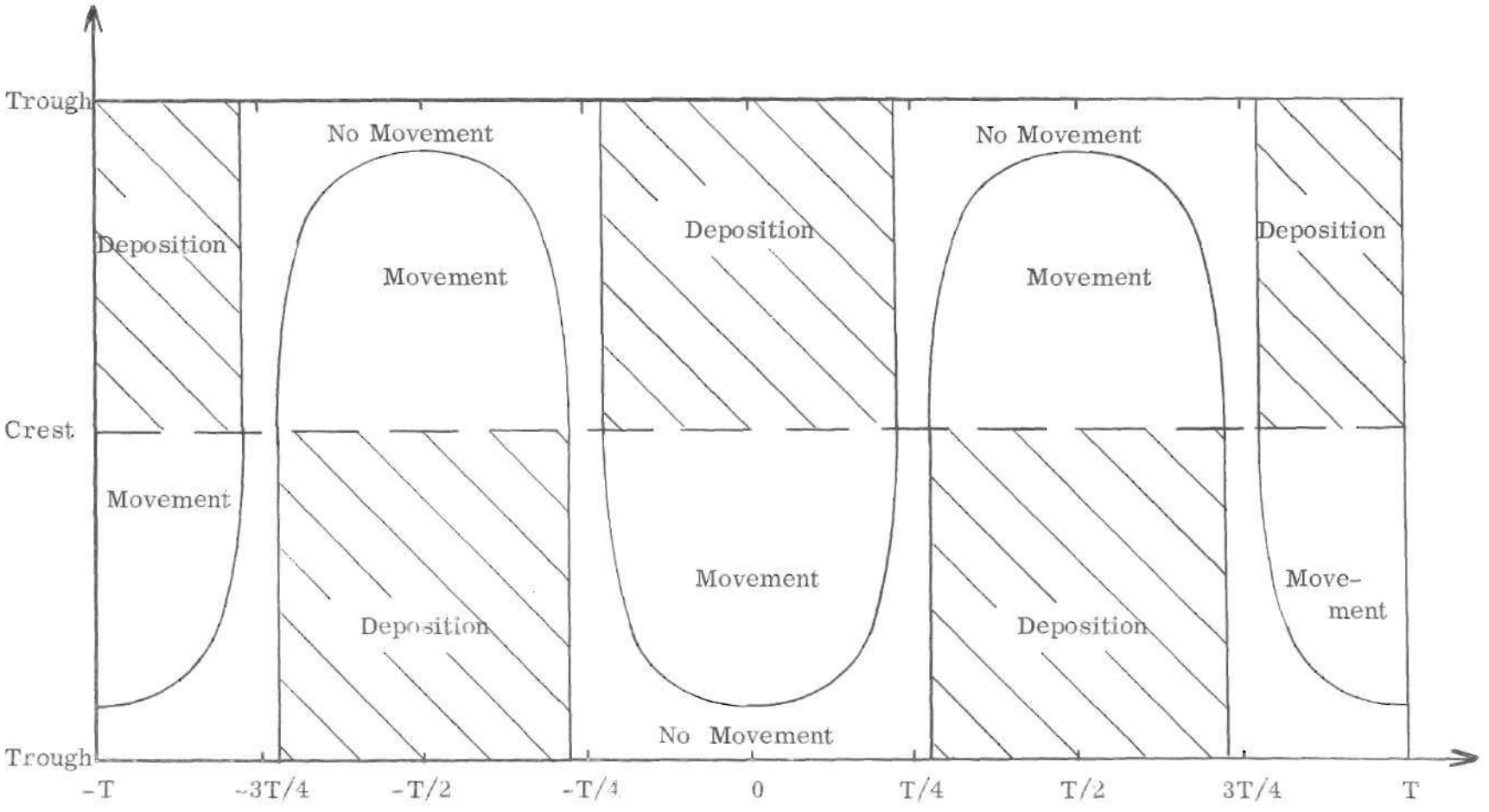

Figure 6. The x-t Plane.

of "movement" and "no movement" in the x-t plane, as previously shown in Figure 6, describe the transport conditions along the upstream face of the dune.

A section of the x-t plane, depicting the upstream face of the crest during one half-cycle of water motion, is shown in Figure 7. The values, u_c/U_m equal 0.2 and a/λ equal 1.0, describe the bed-material properties and the water-motion characteristics considered in Figure 7.

In Figure 7 the line $\overline{oo}$, which is located at x equal zero, is the trough of the dune and the line $\overline{cc}$, which is located at x equal $\lambda/2$, is the crest of the dune. The line $\overline{mm}$, which is determined by means of equation 4, separates the regions of "movement" and "no movement" during the half-cycle. The point $\underline{a}$ is located at the least value of x, x_a, at which scour occurs. Since $\underline{a}$ is located along the line $\overline{mm}$ and since the water-motion velocity at location x_a is a maximum, equation 3 with t_a equal zero, the value of x_a is determined by means of equation 4. The points $\underline{c1}$ and $\underline{c2}$ are located at the time, t_{c1}, at which erosion starts and at the time, t_{c2}, at which erosion ceases, respectively. Since $\underline{c1}$ and $\underline{c2}$ are located along the line $\overline{mm}$ and since both x_{c1} and x_{c2} equal $\lambda/2$, the values of t_{c1} and t_{c2} are also determined by means of equation 4.

The curves $\overline{nn}$, $\overline{pp}$, and $\overline{qq}$ in Figure 7 are three particle paths in the x-t plane; that is, these curves are the displacement-time coordinates of moving sediment particles. If these particles are assumed to move with the fluid, the slope, dx/dt, of a particle displacement curve, such as $\overline{nn}$, $\overline{pp}$, or $\overline{qq}$ is the velocity, u, or

$$\frac{dx}{dt} = \frac{2.4xU_m}{\lambda} \cos \frac{2\pi t}{T} \qquad (6)$$

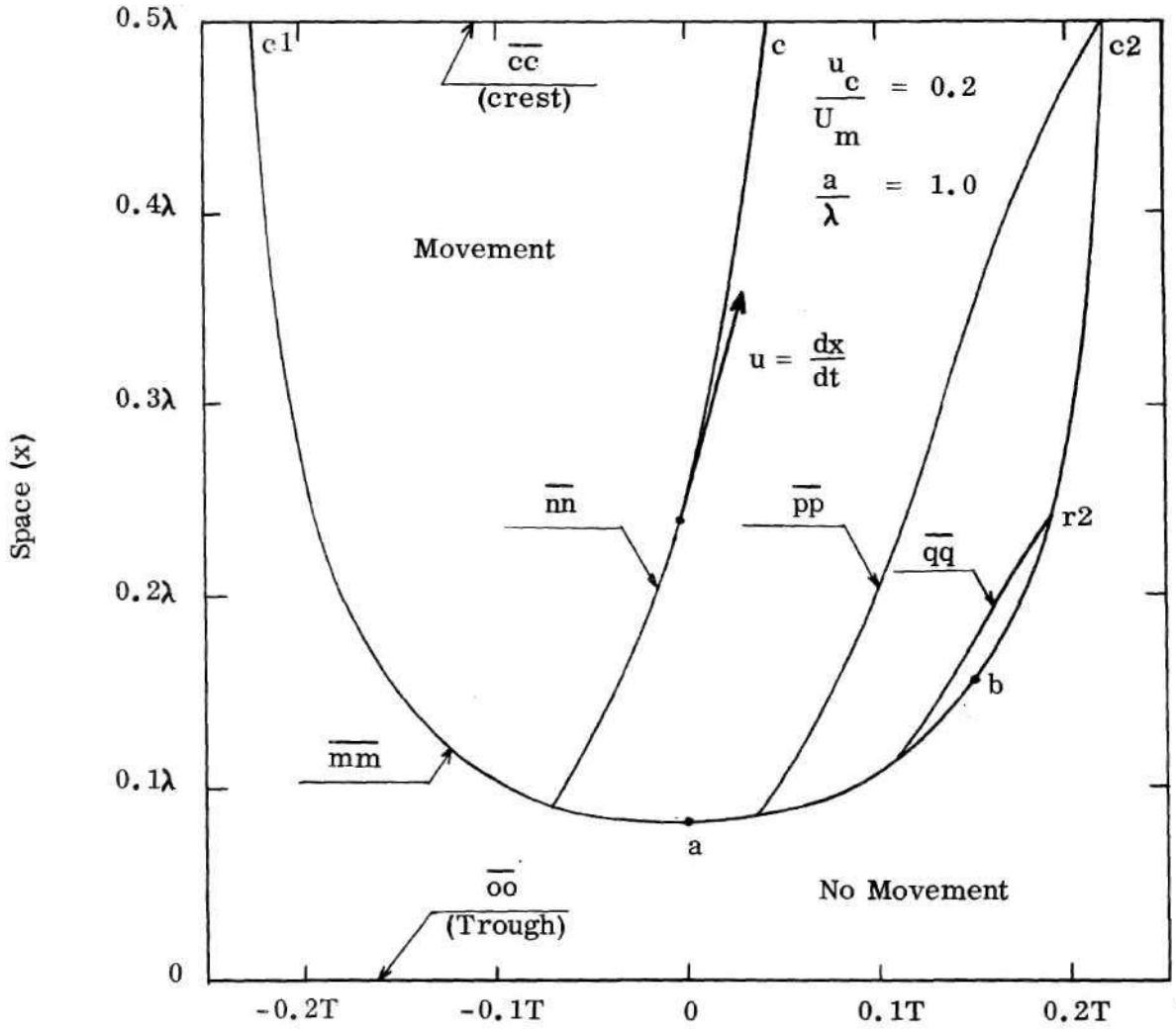

Figure 7. The x-t Plane (Upstream Face).

Equation 6 is a separable differential equation. Integrating equation 6

$$\ln\left(\frac{x_2}{x_1}\right) = \frac{2.4a}{\lambda}\left[\sin\left(\frac{2\pi t_2}{T}\right) - \sin\left(\frac{2\pi t_1}{T}\right)\right] \qquad (7)$$

The initial and terminal points in the integration are (x_1, t_1) and (x_2, t_2) respectively. Equation 7 describes the particle displacement curves in the x-t plane.

Any particle picked up at any location and time along a particular displacement curve will remain on that displacement curve. Each displacement curve, such as $\overline{nn}$, $\overline{pp}$, and $\overline{qq}$ in Figure 7, originates from a point located on an incipient-motion curve, such as $\overline{mm}$ in Figure 7.

Each particle eroded during the half-cycle of water motion is moved along the displacement curve towards the crest of the dune. Most of the particles pass over the crest, however, some particles are deposited along the upstream face before reaching the crest. These two situations are demonstrated in Figure 7. All particles picked up at locations and times along the curve $\overline{nn}$ remain in the region of "movement" until they reach the crest, $\overline{cc}$. Consequently these particles pass over the crest. All particles picked up at locations and times along the curve $\overline{qq}$ pass out of the region of movement and into the region of no movement before they reach the crest. In other words, these particles are deposited on the upstream face. The deposition occurs at the intersection of the particle displacement curve $\overline{qq}$ and the incipient motion curve $\overline{mm}$; that is, at r2. Thus the region of movement in the x-t plane contains two sub-regions; one sub-region contains particles which pass over the crest and the other sub-region contains particles which are deposited along the upstream face.

The last sediment particles passing the crest do so at time t_{c2}; that is, they are located, in space and time, on the displacement curve which passes through the point c2 in Figure 7. Consequently, this particular particle displacement curve, $\overline{pp}$ in Figure 7, separates the two previously mentioned sub-regions. Particles located in the region of movement to the left of $\overline{pp}$ pass over the crest whereas particles located in the region of movement to the right of $\overline{pp}$ are deposited along the upstream face.

The point b in Figure 7 designates the value of x beyond which deposition occurs on the upstream face. In other words, no deposition occurs for any $x<x_b$ and deposition occurs where $x>x_b$. The deposition between x_b and x equal $\lambda/2$ occurs during the time interval from t_b to t_{c2}. The location of b in the x-t plane is established by two conditions. First, the sediment particle at b is in an incipient motion condition and, therefore, lies on the curve $\overline{mm}$ defined by equation 4. Second, inasmuch as any decrease in velocity, u, from the critical velocity, u_c, will result in deposition, the total derivative, du/dt, is equal zero at b and is less than zero between b and c2. Since u is a function of both x and t, the total derivative is as follows,

$$\frac{du}{dt} = u \frac{\partial u}{\partial x} + \frac{\partial u}{\partial t} \qquad (8)$$

Performing the operations shown in equation 8 on equation 3 and letting du/dt equal zero results in the following relationship,

$$\sin\left(\frac{2\pi t_b}{T}\right) = \frac{2.4a}{\lambda}\cos^2\left(\frac{2\pi t_b}{T}\right) \tag{9}$$

Equation 9 is a solution for t_b. The solution for x_b is obtained from equation 4 using the value of t_b obtained from equation 9.

E. Pickup Velocity

In order to evaluate the erosion along the upstream face of the dune, an expression relating the local rate of erosion to the local fluid velocity, u, at particle level and to the bed-material and fluid properties is required. Consequently a pickup velocity u_e, which describes the volume rate of erosion per unit area of bed, is introduced. The pickup velocity is a volume (including both sand grains and voids) transport velocity and may be visualized as the rate at which the bed surface recedes as sediment grains are scoured from the bed.

As an illustration of pickup velocity a cross-section of an eroding sediment-bed is shown in Figure 8. The surface of the bed is inclined at the angle θ to the horizontal. The fluid velocity, u, is tangential to the surface of the bed whereas the pickup velocity, u_e, is normal to the surface of the bed and directed into the bed material. The celerity, $\frac{d\delta}{dt}$, of the surface of the bed is as follows.

$$\frac{d\delta}{dt} = \frac{u_e}{\sin\theta} \tag{10}$$

Obviously, in order to determine the displacement of the bed surface by means of equation 10, the pickup velocity u_e must be known. The removal and

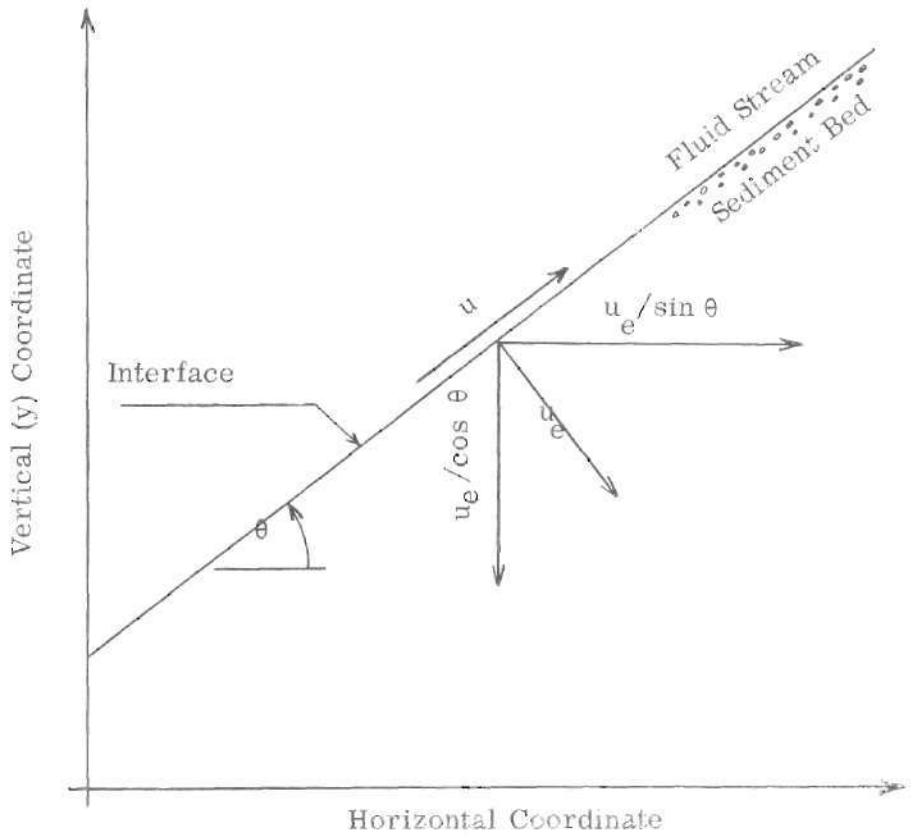

Figure 8. Definition Sketch -- Pickup Velocity.

transport of sediment particles is a complex phenomena for which a theory is non-existent. However, LeFeuvre (10) performed experiments from which an empirical pickup-velocity function can be derived.

LeFeuvre studied the pickup and removal of bed material from an area in the bottom of a 3-in. diameter, horizontal, transparent, plastic pipe. Bed material was forced into the 3-in. pipe through a 1-in. diameter, vertical, copper, water tube. The bed pickup area formed by the intersection of the 1-in. diameter cylinder and the 3-in. diameter cylinder is circular in plan view and is an insular arc in longitudinal cross section. Sands were forced upward by means of a piston in the 1-in. tubing beneath the sand. The piston was moved upward at a uniform rate. Using various combinations of gears the piston speed (sediment-feed rate) could be varied over a hundredfold range in finite increments. The centerline of the opening (pickup area) in the 3-in. pipe was 2 inches downstream from an axially symmetric elliptical contraction by which the flow passage diameter was reduced from 6 inches to 3 inches. Discharge through the 3-in. pipe was controlled by means of a downstream pinch valve and was measured by means of a calibrated V-notch weir.

During a run LeFeuvre established a known sediment-feed rate by selection of gears in the piston-drive mechanism and then adjusted the water discharge to a reference condition. The water discharge was adjusted until the bed particles extended one-half inch downstream from the downstream edge of the supply-tube opening. LeFeuvre states

This single layer of sediment particles was able to stay on the smooth plexiglass tube because it was sheltered from the main flow by the mound upstream from it. The length of this extension bed was, therefore, a sensitive indicator of the height of the mound at the mouth of the supply tube.

LeFeuvre measured velocity distribution at the cross section where the pickup occurred. Velocity distributions without sediment transport were determined by means of a movable stagnation tube with air flowing through the 6-in. approach pipe, the elliptical contraction, and the 3-in. test section. Based on these measurements, LeFeuvre found that the approach velocity profile could be approximated as that for flow over a smooth plate provided that the mean velocity was used for the velocity of infinity and that a distance of 0.41 feet was used as the equivalent length of flat plate.

Because of the unknown height of the mound of sediment at the mouth of the supply tube, the velocity distribution over the mouth of the supply tube is unknown even though the approach-velocity distribution is known from measurements. In analyzing the data, the assumption was made that equation 5 is a universal incipient-motion criterion. Using equation 5 and the properties of the sediments used by LeFeuvre, a value of the incipient velocity u_c could be calculated for each sediment. LeFeuvre tabulated the flow characteristics at an observed incipient-motion condition. The velocity u_c calculated from equation 5 was found to be at a distance from $1.7\ D_g$ to $2.7\ D_g$ from the smooth wall in the approach velocity profile. These values appear to be reasonable inasmuch as any mounding would certainly alter the approach velocity profile tending to bring higher velocities closer to the boundary. In the analysis of LeFeuvre's data, the fluid velocity u at particle level was taken as being the velocity in the approach

velocity profile at a distance of 2.2 D_g from the smooth wall.

LeFeuvre's experiments may be described in terms of pickup velocity. In each of these experiments the bed material was raised at a particular speed such that the surface of the bed remained at a constant elevation. Consequently a measured piston-speed is equal in magnitude, but opposite in direction, to the corresponding pickup velocity. LeFeuvre's experiments were performed with water being the fluid and with six different sediments. The experimental observations show that the pickup velocity u_e is dependent on the flow velocity u at particle level and on the bed-material properties.

In evaluating, from LeFeuvre's observations, an empirical function for pickup velocity, the velocity ratio u_e/u was assumed to be a function of the local sediment number, $N_s = (u/\sqrt{(s-1)\,g\,D_g})$, and the parameter, $1-(u_c/u)^2$. The parameter, $1 - (u_c/u)^2$, is zero when the velocity is equal to u_c. Further the effect of this parameter becomes negligible when $u \gg u_c$. LeFeuvre's data were calculated in terms of the parameters u_c/u, N_s, and $1 - (u_c/u)^2$. Using a numerical procedure for least-squares multiple-regression analysis, the following function was found to be a reasonable representation of LeFeuvre's data

$$\frac{u_e}{u} = 10^{-4} N_s^{\,4} \left[1 - \left(\frac{u_c}{u}\right)^2\right]^{10} \tag{11}$$

Equation 11 is shown in Figure 9 along with LeFeuvre's experimental results.

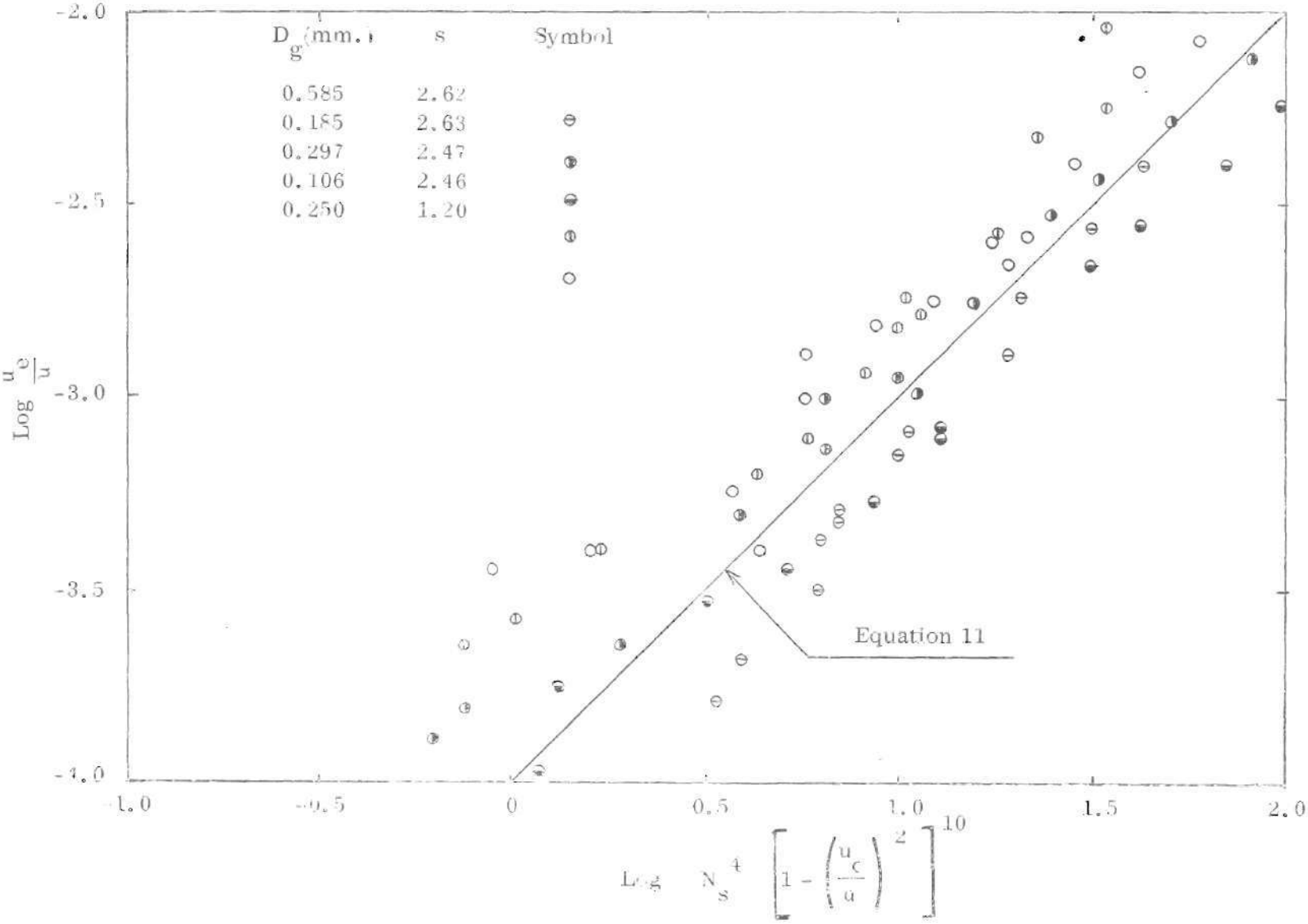

Figure 9. Pick up Velocity.

F. Erosion and Deposition

The regions of the bed, over which erosion occurs, are variable in time and space. As shown in Figure 7, the area being eroded, along the upstream face of each dune, expands and contracts during the half-cycle of water motion. The time interval, during which erosion occurs at a particular location along the upstream face, is also shown in Figure 7.

The regions of the bed, over which deposition occurs, are also variable in time and space. Sediment particles are deposited along the upstream face of the dune whenever the local fluid velocity decreases to the threshold velocity. Consequently the area of the upstream face of each dune over which deposition occurs during each half cycle consists of a particular reach, x_b to $\lambda/2$ in Figure 7, of the dune profile. The specific time at which sediment particles are deposited at any particular location along the upstream face is determined by means of equation 4.

Of course there is a major change in the regions of the bed eroded and the regions of the bed over which deposition occurs every half-cycle. That is, each dune face alternates periodically between being an upstream face, which is primarily an area of scour, and being a downstream face, which is an area of fill. This periodic alternation has been shown in Figure 6.

One consequence of these changes in the areas of scour and fill is a variable dune profile; that is the shape of each dune changes during a cycle of water motion. A change in the dune profile influences the velocity distribution, equation 3, along the upstream face and also the incipient-motion velocity, equation 5, of the

surface particles along the upstream face. However, for small changes in shape, the movement of the face may be considered to be a horizontal shifting of points on the dune profile. For this situation the effects of a change in location of the upstream face are compensated for by allowing the x-y coordinate system to shift horizontally. The movement is such that a point on the profile at elevation y_r remains at the position x_r regardless of the time in the half cycle. The movement of the dune profile and the determination of erosion and deposition along the upstream face are discussed in detail in the following sections.

1. Movement of the Dune Profile

Movement of the profile is illustrated in Figure 10. The profile which exists at the start, t equal -T/4, of the half cycle is asymmetric as shown in Figure 10. This initial profile is unaltered during the time interval $-T/4<t<t_{c1}$; that is, the profile persists until an incipient-motion condition occurs at the crest. After time t_{c1}, however, scouring action along the upstream face of the crest tends to shift the profile horizontally. Two locations of the dune profile, subsequent to the initial location, are shown, in Figure 10, as dashed lines. These profiles are moving during the time intervals shown. That is, during the time interval $t_{c1} < t < 0$, the area over which scour occurs on the upstream face is increasing whereas, during the time interval, $0 < t < t_{c2}$, the area over which scour occurs is decreasing. The fourth location of the dune profile shown in Figure 10 occurs at the time, t_{c2}, at which an incipient motion condition again exists at the crest. During the time interval $t_{c2} < t < T/4$, no scour occurs along the upstream face and the fourth profile persists to the end of the half-cycle.

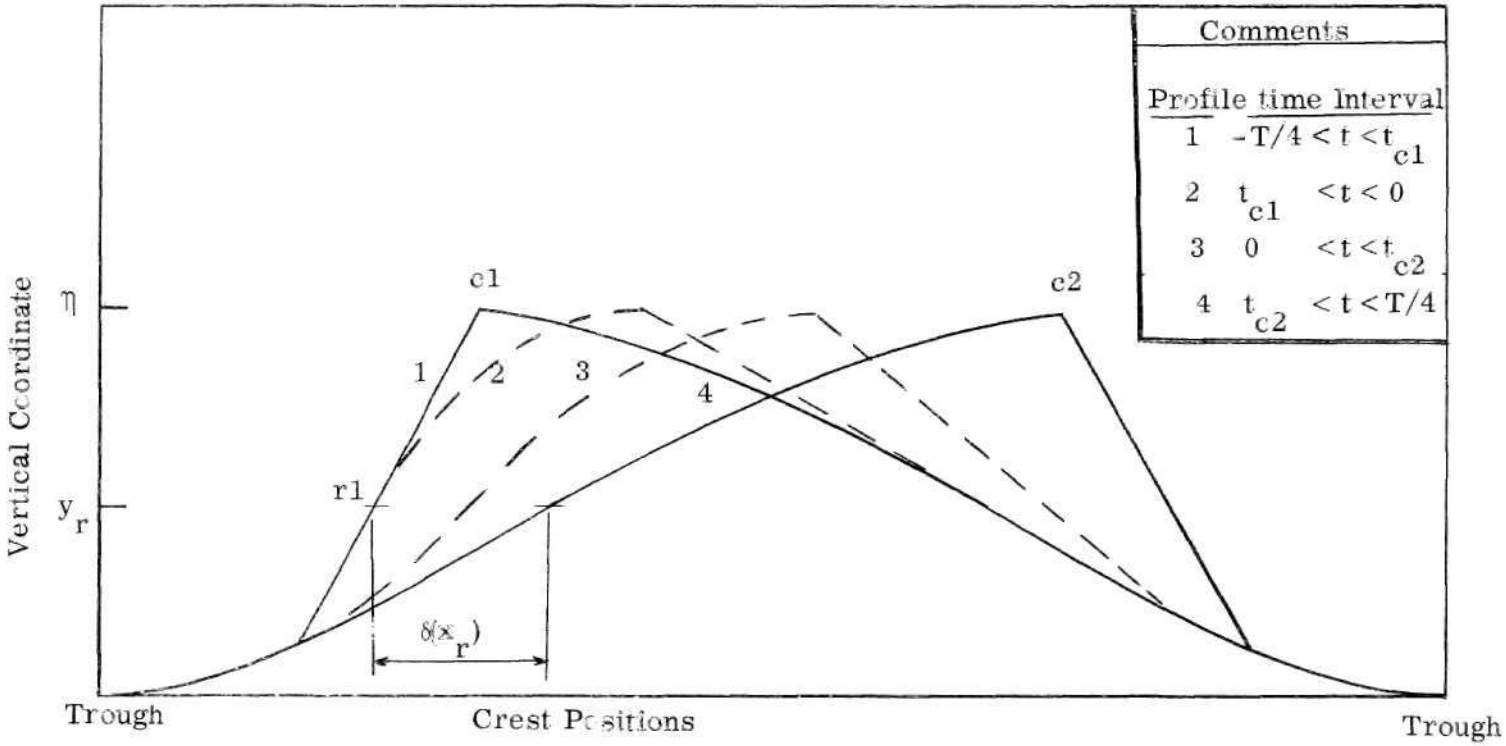

Figure 10. Movement of the Dune Profile.

The least value of x at which scour occurs is x_a as previously shown in Figure 7. For values of x in the range $x_a < x \leq \lambda/2$ the upstream face of the crest is moved horizontally a distance $\delta(x)$. For example, in Figure 10 a point at the elevation y_r, and location x_r, is displaced a distance $\delta(x_r)$. Obviously for values of x in the range $0 < x < x_a$ the value of $\delta(x)$ is zero.

Details of the displacement of the upstream face of a dune are shown in Figure 11. At the beginning of scour, t_{r1}, the dune is at the position shown on the left in Figure 11. At the end of scour, t_{r2}, the dune has moved to the position shown on the right in Figure 11. At any time t, $t_{r1} < t < t_{r2}$, the dune is being eroded at the rate $u_e(x_r, t)$ normal to the upstream face. At the time, t_{r2}, deposition may occur at x_r causing the face to move from r2′ to r2, Figure 11.

From equation 10, the horizontal movement, $\delta_e(x_r)$ in Figure 11, due to erosion at the location x_r during the one-half cycle of water motion is

$$\delta_e(x_r) = \int_{t_{r1}}^{t_{r2}} \frac{u_e(x_r, t)}{\sin \theta} \, dt \qquad (12)$$

Equation 12 is simplified by assuming the change in slope at the location x_r, during the half cycle, is small; that is $\theta \simeq \theta(x_r)$. For this situation the integral in equation 12 may be evaluated numerically*, for a particular bed material, in

- - - - - - -

*The exact solution of the definite integral, equation 12, is cumbersome due to the formulation of the expression, equation 11, relating the pickup velocity to the local fluid velocity. The integral is solved and presented in Appendix A.

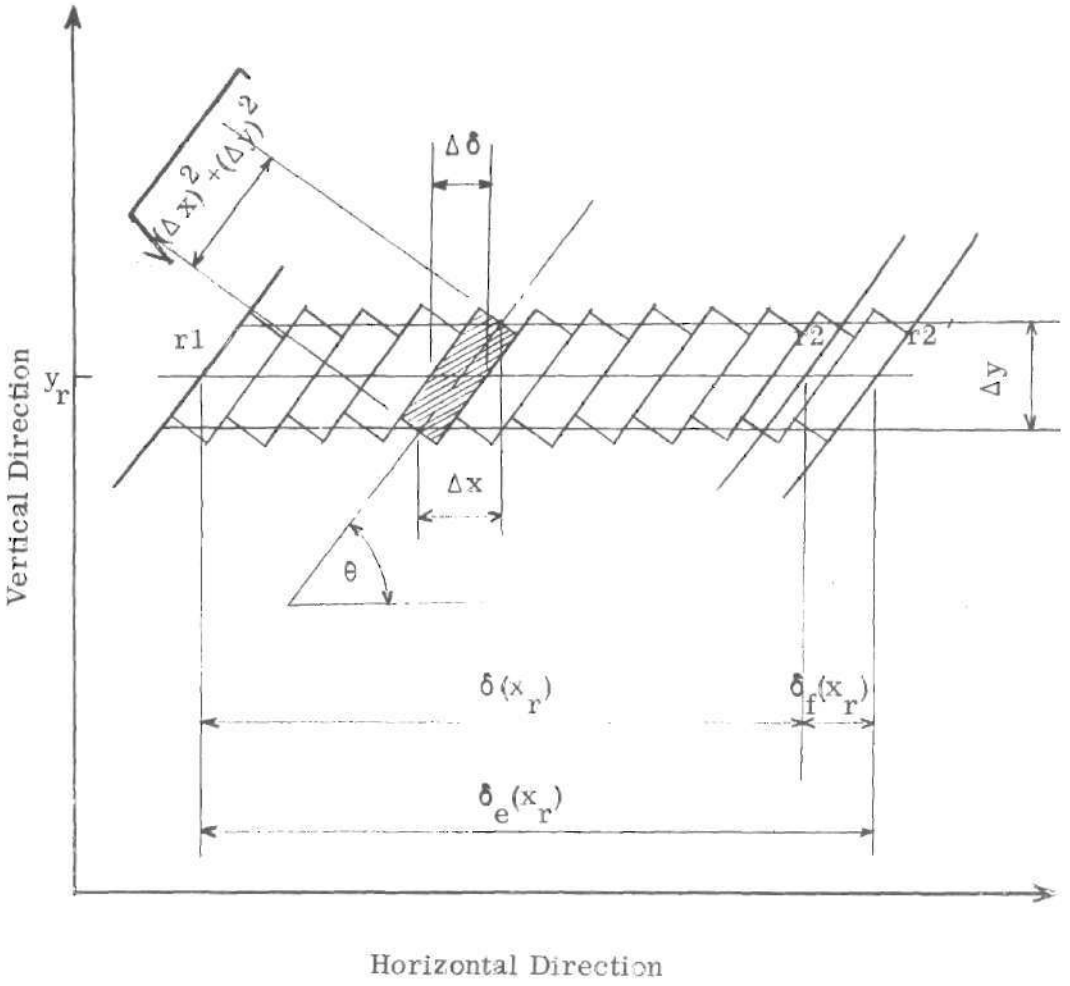

Figure 11. Movement of the Upstream Face.

the form

$$\delta_e(x_r) \sin \theta(x_r) \approx \sum_{i=1}^{\beta} u_e(x_r, t_i)\, \Delta t_i \tag{13}$$

in which β is the number of Δt's into which the entire time is divided; that is, for a constant $\Delta t_i = \Delta t$,

$$\beta = \frac{t_{r2} - t_{r1}}{\Delta t} \tag{14}$$

There is no deposition at the location x_r for x_r in the range $x_a < x_r \leq x_b$. For these locations the net displacement, $\delta(x_r)$ and the displacement, $\delta_e(x_r)$, due to erosion are equal.

There is deposition at x_r when x_r is in the range $x_b < x_r \leq \lambda/2$. For these locations the net displacement is less than the displacement due to erosion by an amount $\delta_f(x_r)$ as shown in Figure 11. That is,

$$\delta(x_r) = \delta_e(x_r) - \delta_f(x_r) \tag{15}$$

In order to evaluate the net horizontal displacement by means of equation 15, the backward movement, $\delta_f(x_r)$, due to deposition at x_r must be known.

A numerical procedure for determining the net horizontal displacement of the location x_r on the upstream face is illustrated in Figure 12. The horizontal line, $\overline{r1r2}$ in Figure 12, represents the summation, equation 13, used to compute the horizontal movement, $\delta_e(x_r)$, due to erosion. The elements along the particle path $\overline{qq}$ represent a summation used to compute the volume of the material deposited

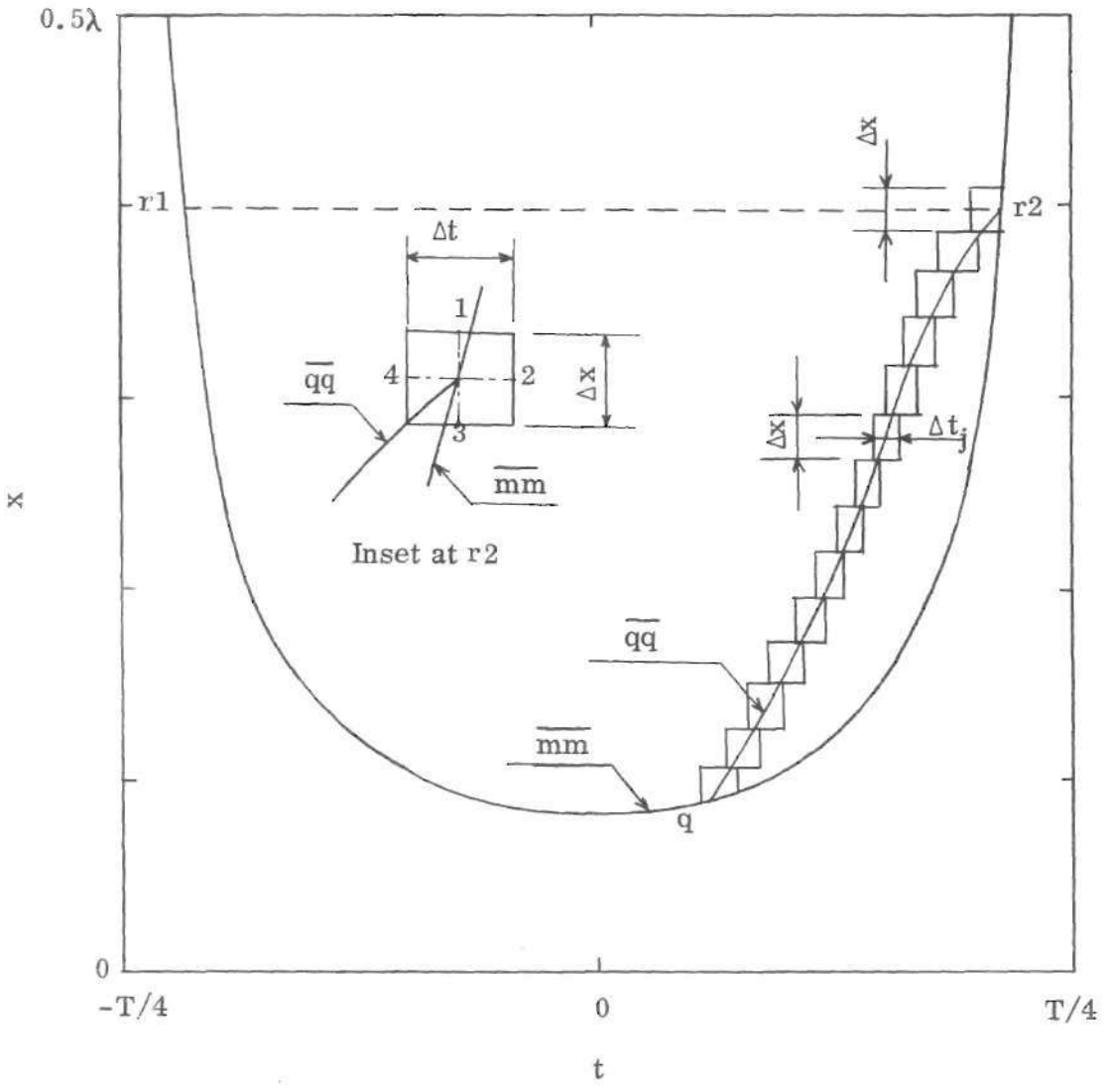

Figure 12. Evaluation of Displacement at Location x_r.

over an area of length Δx at location x_r along the upstream face.

Material is deposited along the upstream face of the crest whenever and wherever the velocity, u, decreases to the threshold velocity, u_c. For example, in Figure 12, all of the sediment grains which have been scoured from the bed along the path $\overline{qq}$ are deposited at r2 since, at r2, u equals u_c. If the distance $x_r - x_q$ is divided into ζ equal-length increments then the small volume of material, ΔV_f, deposited within the Δx increment located at r2 is

$$\Delta V_f = \Delta x \sum_{j=1}^{\zeta} u_e(x_j, t_j)\, \Delta t_j \sqrt{1 + \tan^2 [\theta(x_j)]} \qquad (16)$$

The summation along $\overline{qq}$, equation 16, encompasses the region, in the x-t plane, between two bounding particle paths. The final block, which is the one at r2, is shown in the inset in Figure 12. This block is chosen so that the upper bounding particle-path passes through the points 1 and 4 and the lower bounding path passes through the points 2 and 3. Inasmuch as u equals u_c at r2 the volume eroded from this block equals zero. Using the expression defining the particle paths, equation 7, and the geometry shown in the inset, the following equation relates Δt_ζ to Δx. That is,

$$\Delta t_\zeta = \frac{\Delta x / x_r}{\frac{4.8\pi a}{\lambda T} \cos\left(\frac{2\pi t_{r2}}{T}\right)} \qquad (17)$$

The values of Δt_j, which confine the blocks to the region between the two bounding particle paths, are related to Δt_ζ. That is, using equation 7,

$$\Delta t_j = \frac{\cos \frac{2\pi t_{r2}}{T}}{\cos \frac{2\pi t_j}{T}} \Delta t_\zeta \tag{18}$$

Since the volume deposited within the last Δx increment may be approximated by $\delta_f (x_r)\, \Delta y$ and since $\Delta y/\Delta x$ is an approximation of $\tan [\theta (x_r)]$ the backward movement, using equation 16, at $\underline{r2}$ is

$$\delta_f(x_r) \tan [\theta(x_r)] \approx \sum_{j=1}^{\zeta} u_e(x_j, t_j) \sqrt{1+\tan^2 [\theta (x_j)]}\, \Delta t_j \tag{19}$$

The values of Δt_ζ and Δt_j in equation 19 are determined by means of equations 17 and 18 respectively.

The displacement of the upstream face of a dune profile is determined by means of equations 13, 19, and 15. In order to use these equations the initial shape of the upstream face must be known; that is the variable $\theta (x_r)$ must be known. A reasonable (typical) profile has been presented previously in Figure 5.

The total volume eroded, the total volume deposited, and the net volume removed from the upstream face during one-half cycle may be evaluated from the displacements $\delta_e(x)$, $\delta_f(x)$, and $\delta(x)$ respectively.

That is

$$V_e = \int_{x_a}^{\lambda/2} \delta_e(x) \tan [\theta(x)]\, dx \tag{20a}$$

$$V_f = \int_{x_b}^{\lambda/2} \delta_f(x) \tan [\theta(x)] \, dx \tag{20b}$$

and

$$V = \int_{x_a}^{\lambda/2} \delta(x) \tan [\theta(x)] \, dx \tag{20c}$$

It is, of course, convenient to evaluate equations 20a, b, and c numerically.

2. Volume Rate of Transport

The volume rate of transport, $q_s(x,t)$, is the volume rate of transport per unit length of crest passing the location x at time t. The method of determining the volume rate of transport at the position x_r and time t_r are illustrated in Figure 13.

Sediment particles are picked up along particle paths, such as $\overline{nn}$ in Figure 13, and move along the upstream face of the dune towards the crest. Particles picked up along $\overline{nn}$ between the points $\underline{n}$ and $\underline{r}$ pass the position x_r at the time t_r. In Figure 13 the distance $x_r - x_n$ is divided into ζ equal-length increments. The particles picked up along $\overline{nn}$ between $\underline{n}$ and $\underline{r}$ pass x_r during the time interval Δt_ζ. Since equation 16 evaluates the volume eroded along a particle path, the volume rate of transport at position x_r and time t_r is

$$q_s(x_r, t_r) = \frac{\Delta x}{\Delta t_\zeta} \sum_{j=1}^{\zeta} u_e(x_j, t_j) \, \Delta t_j \sqrt{1 + \tan^2 [\theta(x_r)]} \tag{21}$$

Since the summation, equation 21, encompasses a region between two bounding

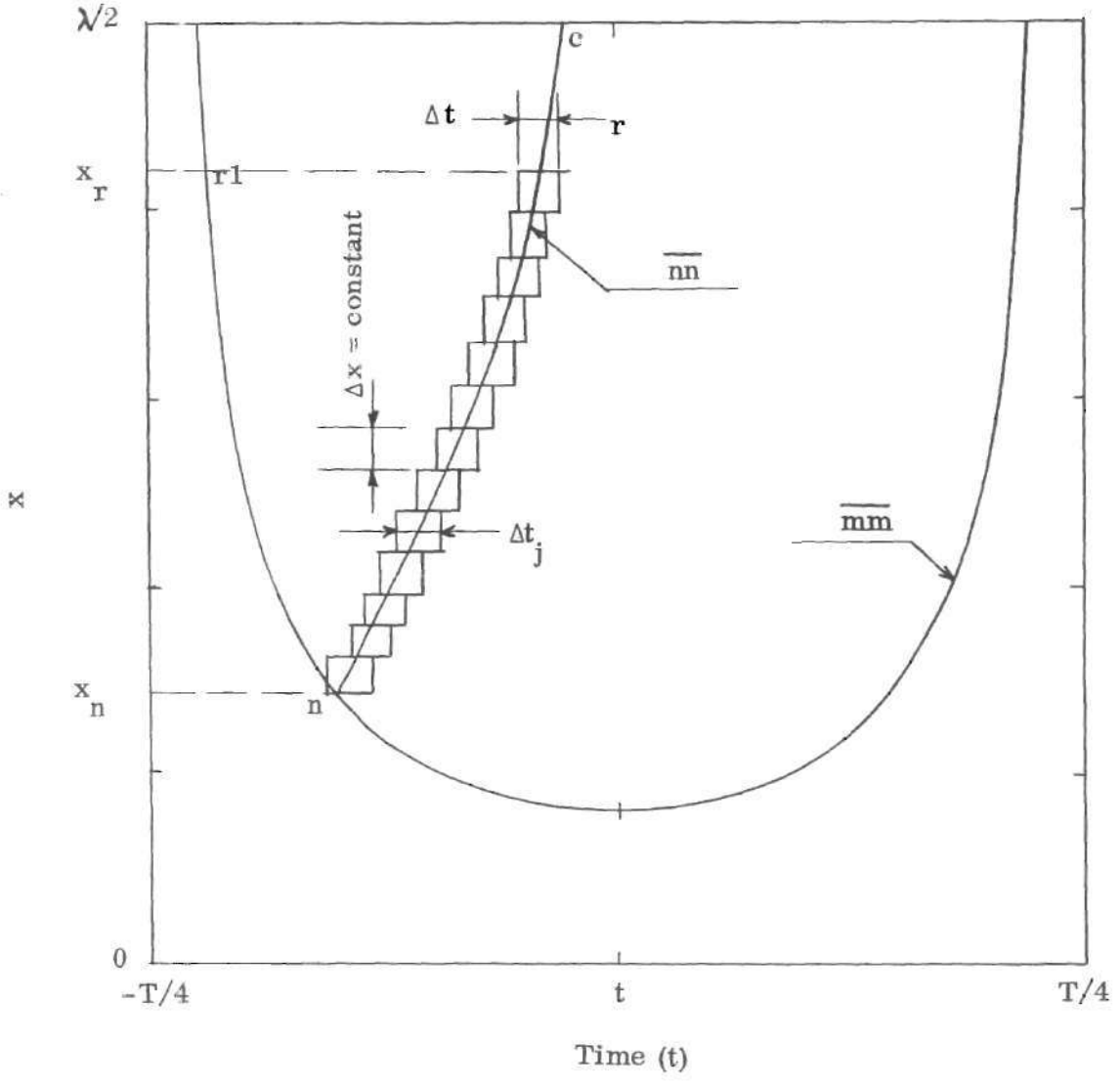

Figure 13. Evaluation of Volume Rate of Transport.

particle paths, in the same manner as the earlier summation (equation 16), the values of Δt_j are related to Δt_ζ by equation 18.

The volume rate of transport over the crest may be evaluated by means of equation 21. For example, the value of $q_s\ (\lambda/2, t_c)$, Figure 13, is obtained by means of equation 22 when ζ equal the number of equal-length increments in the length $\lambda/2 - x_n$, x_r equal $\lambda/2$, and t_r equal t_c.

The net volume, V, passing the crest may be evaluated by integrating the volume rate of transport over the crest with respect to time. In other words

$$V = \int_{t_{c1}}^{t_{c2}} q_s\ (\lambda/2, t)\ dt \qquad (22)$$

Equation 22 is evaluated numerically. Of course the value of V obtained by means of equation 22 and the value of V obtained by means of equation 20c are equal.

CHAPTER III

THEORETICAL ANALYSIS

A. Introduction

The variables that govern erosion processes along a duned bed consist of the bed-material properties, the fluid properties, and the variables which describe the fluid motion. The foregoing theory describes, in space and time, erosion and deposition along the upstream face of a dune in terms of any reasonable combination of these fluid, bed material, and fluid motion variables. This discussion concerns the evaluation of erosion processes during oscillatory fluid-motion over a duned bed by means of the foregoing analysis.

The computations are simplified in that the slope of the upstream face is assumed to be small. The consequences of this simplification are the following:

$1 + \tan^2 \theta$ is unity in equations 16, 19 and 21; (23a)

$\frac{\tan \phi \cos \theta + \sin \theta}{1 + \tan \phi}$ equals $\frac{\tan \phi}{1 + \tan \phi}$ in equation 5; (23b)

and, $\cos \theta$ is unity in equation 20a. (23c)

The number of variables used in the computations is reduced by considering a particular set of dimensionless parameters. The celerity of the dune face, using equations 10 and 11, is

$$\frac{d\delta}{dt} = \frac{2\pi(10^{-4})\, a u N_s^4}{U_m T \sin\theta} \left[1 - \left(\frac{u_c}{u}\right)^2\right]^{10} \tag{24}$$

For any bed material and fluid-motion u/U_m is equal to N_s/N_{sm} and u_c/u is equal to N_{sc}/N_s. In addition u/U_m is a specific function, equation 3, of space and time. The value of θ is also a function of space and time. Consequently, the variables which must be considered in evaluating equation 25 are included in the following set of dimensionless parameters.

$$\frac{d(\delta/\lambda)}{d(t/T)} = f\left(\frac{a}{\lambda}, \frac{u_c}{u_m}, N_{sc}, \frac{x}{\lambda}, \frac{t}{T}\right) \tag{25}$$

Three parameters $\frac{a}{\lambda}$, $\frac{u_c}{u_m}$, and N_{sc} describe the pertinent bed-material and fluid properties and the fluid motion. The remaining two parameters $\frac{x}{\lambda}$, and $\frac{t}{T}$ are space and time variables expressed in terms of dune wave length and fluid-motion period.

Erosion and deposition along the dune profile are computed in two parts. Firstly, the total volume eroded, the total volume deposited, and the net volume removed from the upstream face during one-half cycle are determined. From these values the relative importance of the deposition along the upstream face is determined. Secondly the volume rate of transport over the crest is determined. From these values the lag between the time of maximum fluid-motion velocity and maximum rate of sediment transport is determined. The computed values are presented in the following.

B. Erosion, Deposition, and Net Volume Removed From the Upstream Face During One-Half Cycle

The total horizontal movement, due to erosion during one-half cycle of fluid-motion, is evaluated by means of equation 12 (or 13) and the sediment pickup function, equation 11. The limits of the integration, equation 12, are dependent, equation 7, on the location being considered and on u_c/U_m. Therefore, considering equation 25, the variables describing the total horizontal movement δ_e are the following.

$$\frac{\delta_e}{\lambda} = \frac{\delta_e}{\lambda}\left(\frac{a}{\lambda}, \frac{u_c}{u_m}, N_{sc}, \frac{x}{\lambda}\right) \tag{26}$$

In equation 26 the parameter a/λ is involved in a known way; that is, linearly according to equation 24. The role of the remaining variables is determined by the summation, equation 13, and the sediment pickup function, equation 11.

The total volume, V_e, eroded from the upstream face during one-half cycle of fluid motion is evaluated by summing elemental volumes, $\delta_e \tan\theta\,\Delta x$, over the complete scoured area. This summation corresponds to the integration shown in equation 21a. The lower limit of the summation is the point x equal x_a, Figure 7, and the upper limit is the crest of the dune, x equal $\lambda/2$. Therefore, considering equation 26, the total volume eroded from the upstream face is

$$\frac{V_e}{\lambda^2} = \frac{a}{\lambda} f_1\left(N_{sc}, \frac{u_c}{U_m}\right) \tag{27}$$

Values of the function, f_1, are shown in Figure 14(a). As shown in Figure 14(a) the relationship expressed by equation 27 may be further reduced; that is

$$\frac{V_e}{\lambda^2} \approx \frac{a N_{sc}^4 f_2 \left(\frac{u_c}{U_m}\right)}{\lambda} \tag{28}$$

Values of the function f_2 are shown in Figure 14(b).

The region, in the x-t plane, containing particles which are swept over the crest is separated from the region containing particles which are deposited along the upstream face by a particular particle-path, $\overline{pp}$ in Figure 7. The coordinates of this particle-path are determined by the coordinates of point c2 and equation 7. Hence, the two parameters, u_c/U_m and a/λ, are necessary in order to delineate the two aforementioned regions. Therefore, using a development similar to equations 24, 25, 26, and 27 and incorporating this additional effect of a/λ and u_c/U_m, the net volume passing the crest during one-half cycle may be expressed in terms of the following dimensionless variables.

$$\frac{V}{\lambda^2} = \frac{V}{\lambda^2}\left(\frac{a}{\lambda}, \frac{u_c}{U_m}, N_{sc}\right) \tag{29}$$

Similarly the volume deposited along the upstream face may be expressed as

$$\frac{V_f}{\lambda^2} = \frac{V_f}{\lambda^2}\left(\frac{a}{\lambda}, \frac{u_c}{u_m}, N_{sc}\right) \tag{30}$$

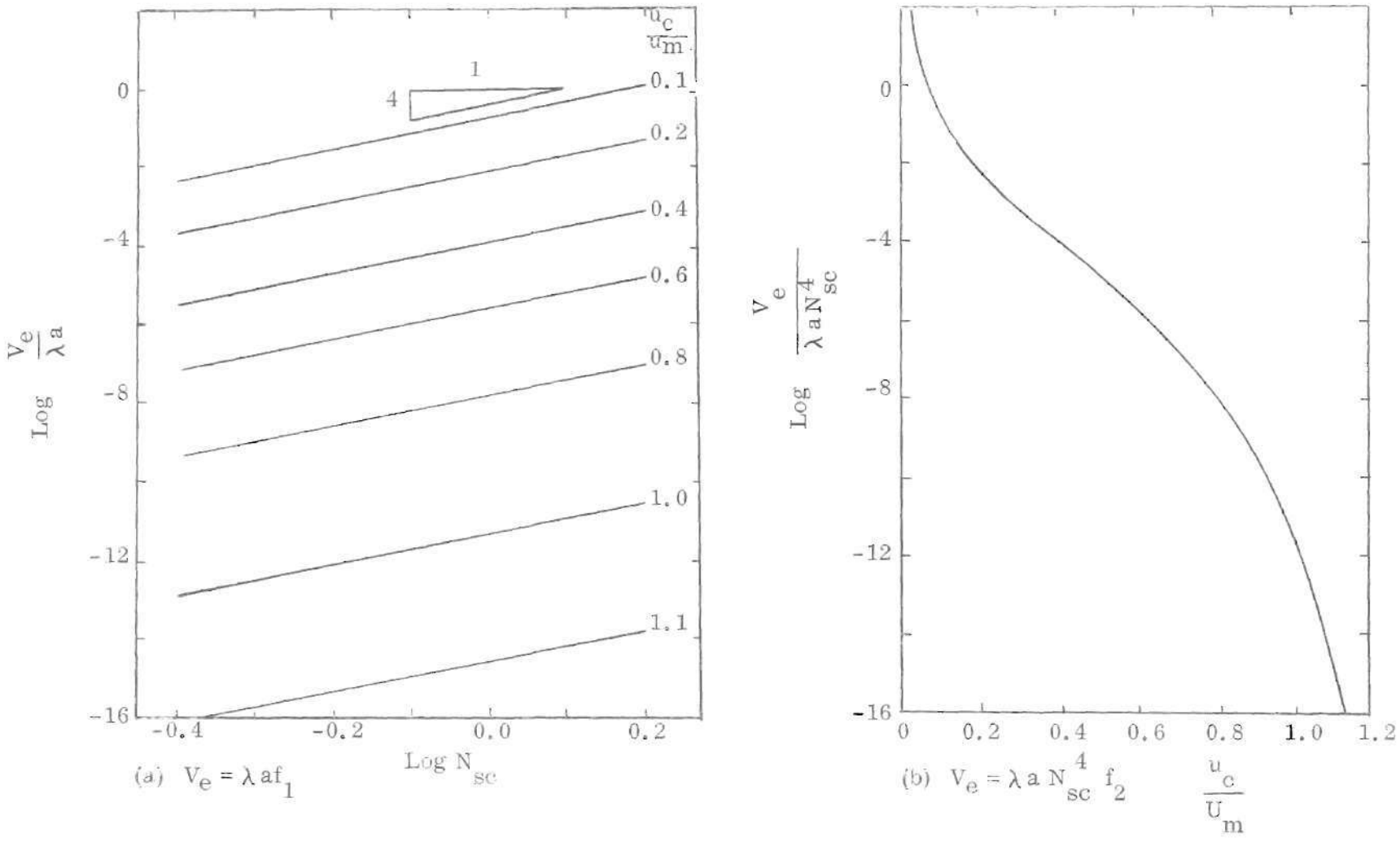

Figure 14. Total Volume Eroded Along the Upstream Face.

There is a range of values of a/λ through which, for a specified maximum fluid-motion velocity and a particular bed material, the deposition along the upstream face is negligible. In other words, when the deposition is small in comparison with the total volume eroded, then the net volume eroded, equation 29, may be considered equal to the total volume eroded, equation 28. The values of the total volume eroded, the volume deposited, and the net volume removed from the upstream face are shown in Figure 15(a), evaluated by numerical integration of equations 20a, b, and c, respectively, for a/λ equal 1.0 and N_{sc} equal 1.0. As shown in Figure 15(a), for these particular values of a/λ and N_{sc}, the deposition is negligible in comparison to the total volume eroded. Five levels of the ratio, V/V_e, of the net volume removed to the total volume eroded, evaluated by numerical integration of equations 20a and c are shown in Figure 15(b) for N_{sc} equal 1.0. As shown in Figure 15(b), for reasonable values of a/λ and u_c/U_m the deposition is, in fact, negligible. For example when u_c/U_m equal 0.2, N_{sc} equal 1.0 and a/λ equal 0.2 then the net volume removed equals 95 per cent, Figure 15(b), of the total volume eroded along the upstream face.

There is a value of a/λ above which, for a specified maximum water-motion velocity and a particular bed material, the deposition along the upstream face is identically zero. Obviously, no deposition occurs when the point b and the point c2, shown previously in Figure 7, coincide. Therefore any point on the curve V/V_e equal 1.0, Figure 15(b), may be located by letting t_b equal t_{c2}, and evaluating a/λ by means of equation 3. The value of a/λ obtained is independent of N_{sc}. Consequently, the level V/V_e equal 1.0 in Figure 15(b), and the region above this level

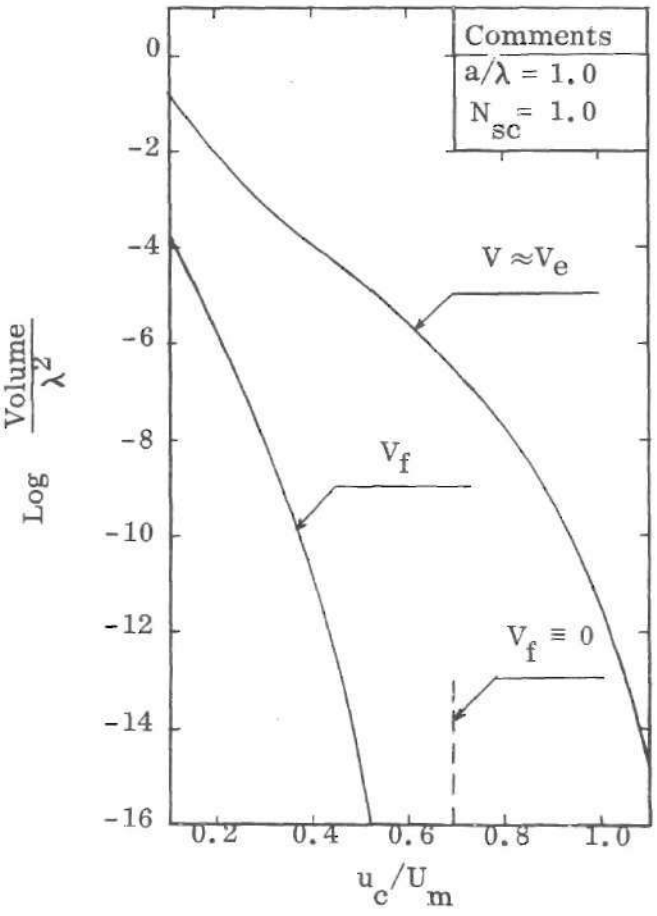

(a) Volume

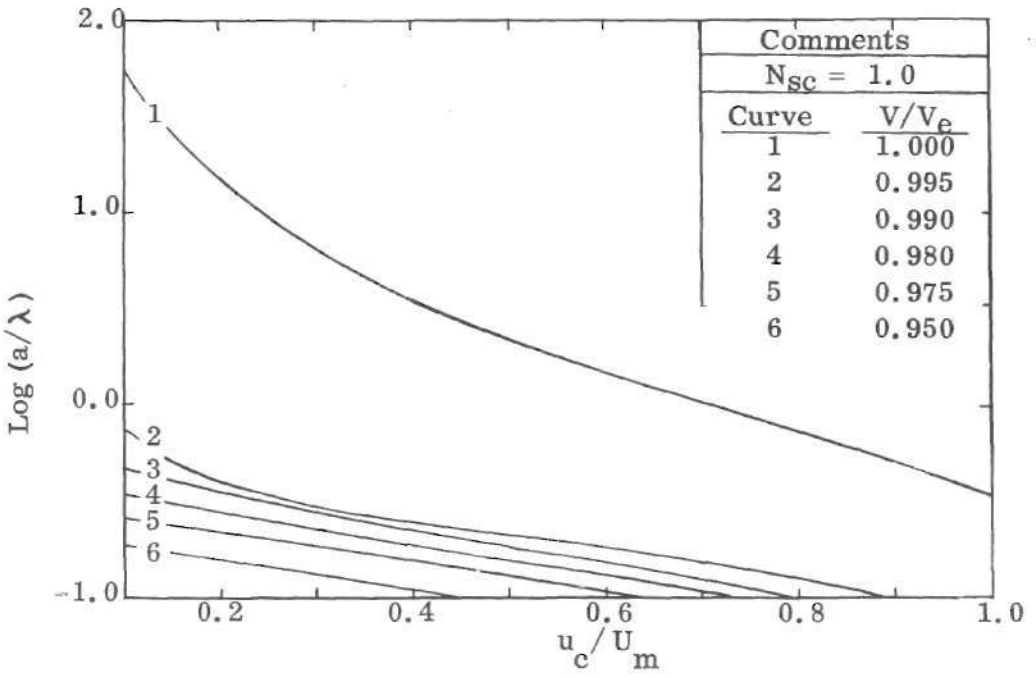

(b) Ratio of Volume Passing the Crest to the Total Volume Eroded

Figure 15. Erosion and Deposition Along the Upstream Face.

(within which $V/\forall_e$ equal 1.0), is independent of N_{sc}.

C. Volume Rate of Transport

The volume rate of transport, $q_s(x,t)$, at the location x along the upstream face and the time t during the half-cycle is evaluated by means of equation 21 and the sediment pickup function, equation 11. The volume rate of transport, $q_s(\lambda/2,t)$, at the crest of the dune is shown in Figure 16 (a, b, c, and d) for a/λ equal 1.0 and selected values of u_c/U_m and N_{sc}. The combination of dimensionless variables presented in Figures 16 (a, b, c, and d) is obtained by means of equations 3, 11, 21, and 24 and may be expressed in the following form.

$$\frac{Tq_s}{\lambda^2} = \frac{Tq_s}{\lambda^2}\left(\frac{a}{\lambda}, \frac{u_c}{U_m}, N_{sc}, \frac{t}{T}, \frac{x}{\lambda}\right) \tag{31}$$

The lag between the time, t equal zero, of maximum water motion velocity and the time, t equal τ, of maximum rate of sediment transport is illustrated in Figures 16(a, b, c, and d). The magnitude of the time-lag depends on the size of the scour region and on the trajectory of the particle paths. The magnitude of the time-lag is independent of the overall intensity of scour; that is, referring to Figures 16 (a, b, c, and d) τ is independent of N_{sc}. Therefore, considering equations 4 and 7, the time-lag may be presented as the following combination of variables.

$$\frac{\tau}{T} = \frac{\tau}{T}\left(\frac{a}{\lambda}, \frac{u_c}{U_m}, \frac{x}{\lambda}\right) \tag{32}$$

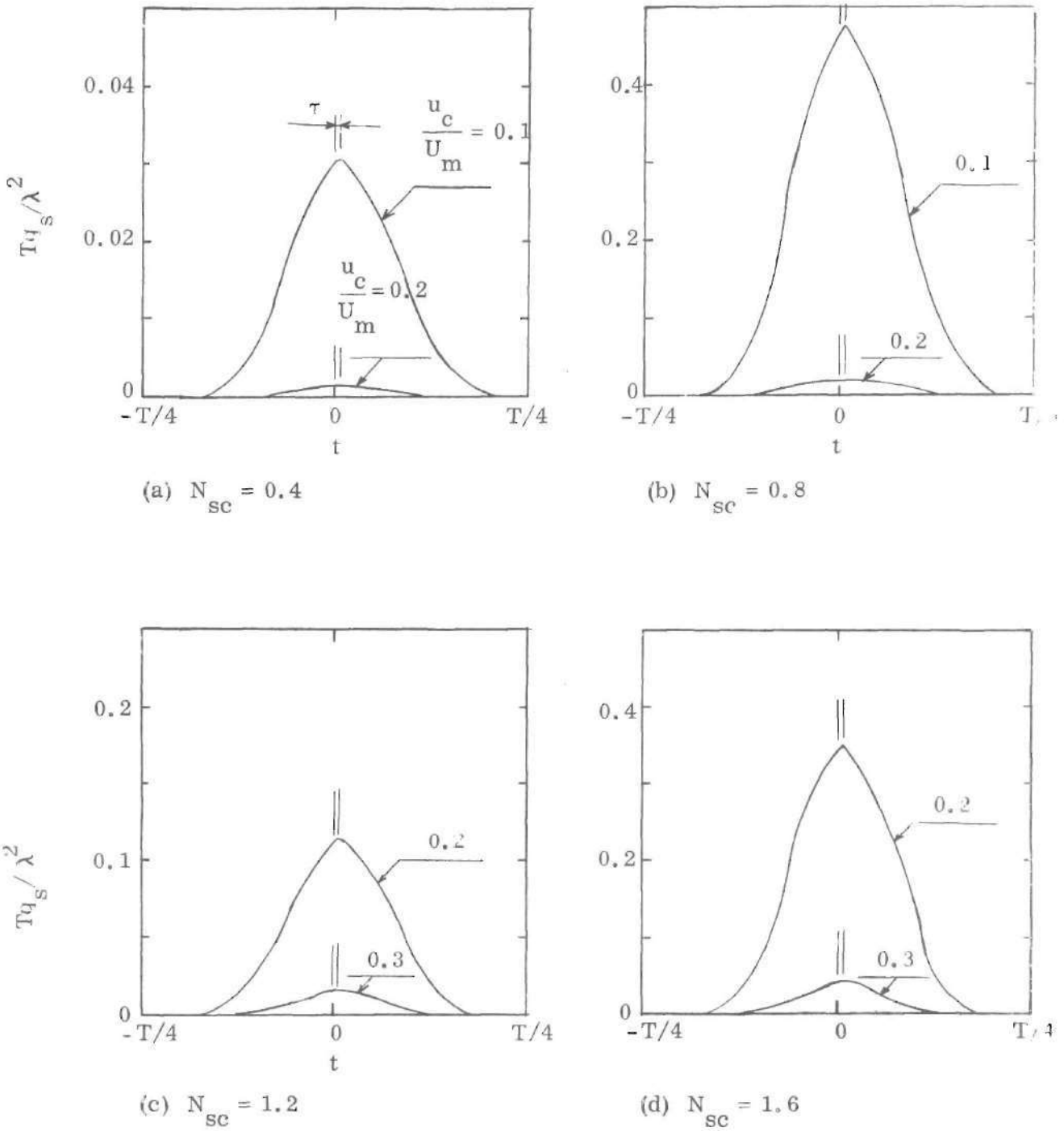

Figure 16. Volume Rate of Transport at the Crest.

The time-lag at the crest, x equal $\lambda/2$, is shown in Figure 17. As shown in Figure 17, the time-lag at the crest decreases towards zero for increasing values of a/λ or u_c/U_m.

D. Movement of the Dune Profile

The net forward movement, evaluated by means of equations 13, 15, and 19 is presented in Figure 18. The value u_c/U_m equal 0.2 was used in the evaluation. The angle θ, which is the slope of the face at a particular value of x_r, is not described by the scour relationships.

As previously shown in Figures 15(a, b) the volume deposited along the upstream face is, for reasonable values of a/λ, u_c/U_m, and N_{sc}, negligible in comparison with the total volume eroded along the upstream face. This is a consequence of the fact that, for similar reasonable values of a/λ, u_c/U_m and N_{sc} the value of the backward movement $\delta_f(x_r)$, due to deposition of x_r is much less than the value of the total forward movement, $\delta_e(x_r)$, due to erosion at x_r. Consequently the net forward movement at location x_r may be considered equal to the total forward movement $\delta_e(x_r)$.

The displacement, $\delta(x_r)$, at any position along the upstream face may be expressed by an approximate relationship. In particular, the movement, δ_c of the dune crest may be approximated by

$$\frac{\delta_c}{\lambda} \approx \frac{a\, N_{sc}^{\,4}}{\lambda \sin\theta} \quad f_3\left(\frac{u_c}{U_m}\right) \tag{33}$$

The development leading to equation 33 is similar to the development leading to

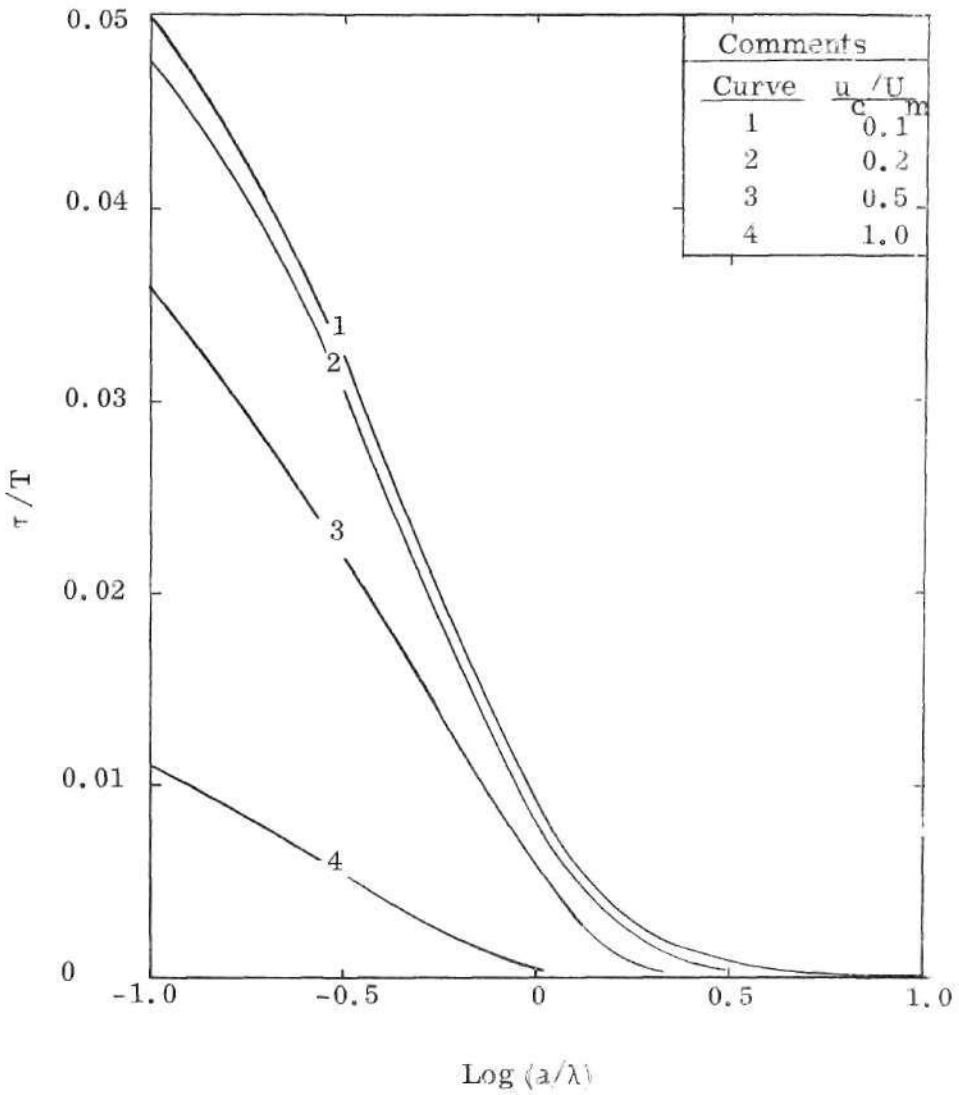

Figure 17. Time-Lag at the Crest.

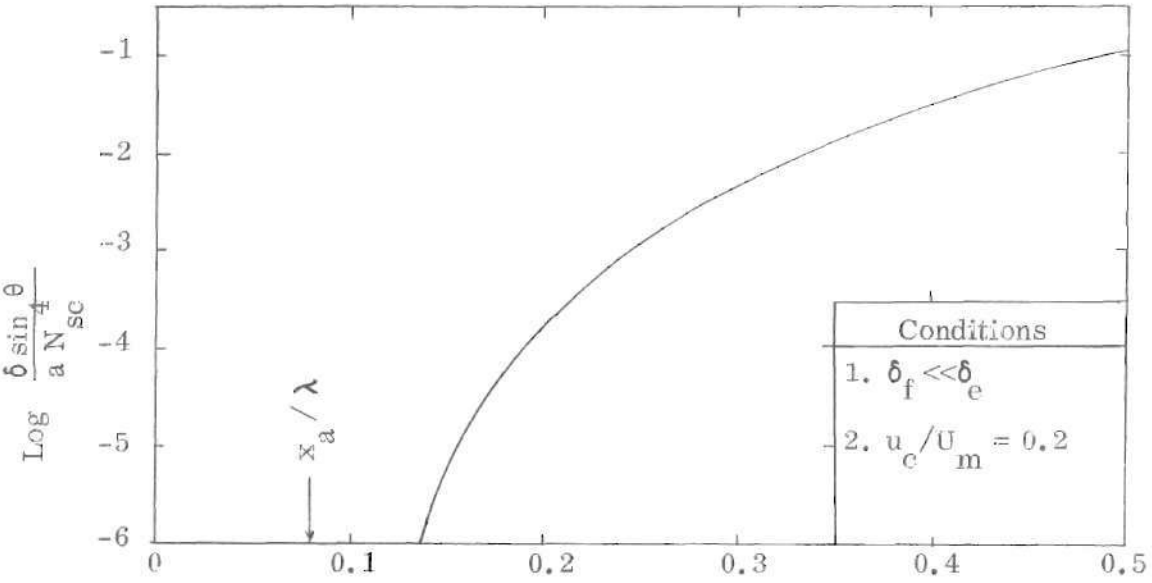

(a) The Upstream Face

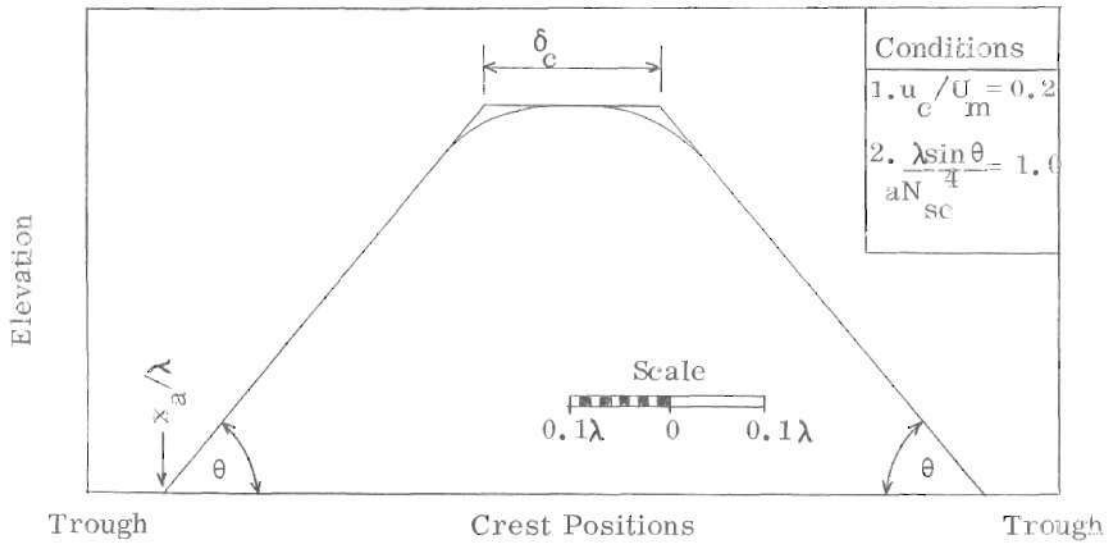

(b) Dune Profiles

Figure 18. Displacement of the Dune Profile.

equation 33 is similar to the development leading to equation 28 and is correct when there is no depositions at the point c2, Figure 7. Consequently equation 33 is applicable when the value of V/V_e, Figure 15(b), is approximately unity; that is, for reasonable values of a/λ and N_{sc}. The value of $f_3 (u_c/U_m)$ is shown in Figure 19.

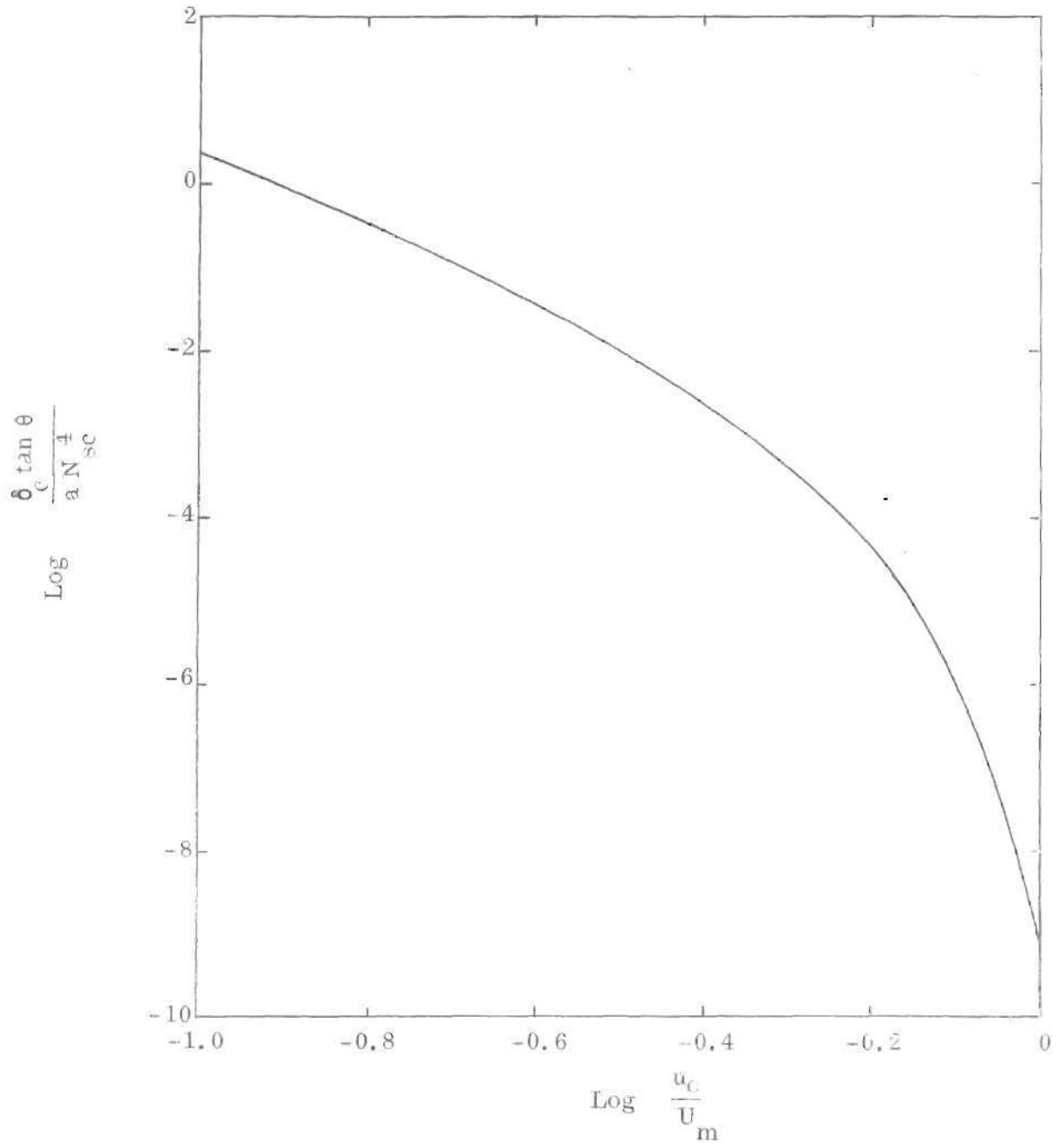

Figure 19. Movement of the Crest.

CHAPTER IV

ANALYSIS AND DISCUSSION OF EXPERIMENTAL OBSERVATIONS

A. Introduction

The analysis describes erosion and deposition along the upstream face of each dune. The development of a duned bed is a consequence of the variation in erosion and deposition along the fluid-sediment interface. An equilibrium or stable interface will occur whenever the volume eroded along the upstream face of a dune is identical, in magnitude and location, to the volume deposited along the same face during the following one-half cycle of fluid motion. The analysis is used herein to obtain parametrical representations of three aspects of a deformed fluid-sediment interface. Firstly the mechanics of development are explained; secondly, the volumes eroded from an equilibrium dune are investigated; and thirdly, the movement of an equilibrium-dune profile is evaluated.

The three above mentioned topics are discussed in the following sections. All quoted experimental data, Appendix B, concerning a deformed fluid-sediment interface were performed with water, having a specific gravity of about unity, as the fluid. Since most natural beach sands have (7) a specific gravity of about 2.65 the value s equal 2.65 is used, where noted in the following discussions, to illustrate particular situations.

B. Development of a Duned Bed

Experimental information regarding the development of a duned bed has been presented by Carstens, Neilson, and Altinbilek (3). These data are, to the writer's knowledge, the only available data which present the comprehensive, history-of-development information needed to describe the growth of a dune system. Consequently, this discussion is restricted to the initial conditions employed in the earlier study; that is, to the development of dunes from an initially plane sediment-water interface.

Obviously the typical dune profile, Figure 5, does not exist on the plane sediment bed at commencement of oscillatory water motion. The first bed forms observed (3) on the interface are rolling-grain features called ripples. The ripple crests accumulate sediment grains until separation occurs at the crest. When separation occurs, a vortex forms in the lee of the crest. The bed form is then termed a vortex feature, or dune, and the erosion may then be evaluated by means of the previous analysis. The ripples are an initial condition leading to the development of dunes.

The surface of an erodible bed, shortly after commencing oscillatory water motion above the bed, has been observed (3) to assume one of four different patterns. These patterns are the following:

(a) a plane immobile bed -- no ripples form, or can be induced to form, on the interface;

(b) induced ripples -- rolling grains occur adjacent to a disturbance in the flow near the bed,

(c) spontaneous ripples -- bands of rolling sediment grains occur simultaneously along the bed surface, and

(d) a plane mobile bed -- the surface of the bed remains plane although the bed-material moves back and forth with the water motion. The ripples, occurrences (b) and (c) above, are initial conditions which necessarily precede the development of a duned bed. In order to investigate the development of the bed, from the first occurrence of dunes to the existence of equilibrium dunes, the initial conditions must be known in terms of the independent variables presented in the analysis.

The wave length, λ_0 at the first occurrence of dunes is unknown. This wave length is established by factors which create a rolling grain feature. Consequently, the initial conditions are typified herein in terms of N_{sc} and u_c/U_m and not in terms of a/λ_0.

The delineation of the types of initial condition, in terms of N_{sc} and u_c/U_m, is shown in Figure 20. The values of N_{sc} and u_c/U_m of the plotted points are computed using equation 5 and published data (3, 7). As stated earlier the calculations use the values: Φ equal 30-degrees (3, 11); θ equal 0-degrees, and g equal 32.2 ft/sec.^{2} The drag coefficient C_D' is from Albertson, Barton, and Simons (11) and is for natural sand particles having a shape factor of 0.7. The delineation of the four regions is as follows.

(a) The lower limit, $\overline{AA}$ in Figure 20, of the mobile plane-bed condition has been investigated experimentally by Manohar (7). His extensive experiments, indicate that this limit, for a particular bed material, is a function of maximum

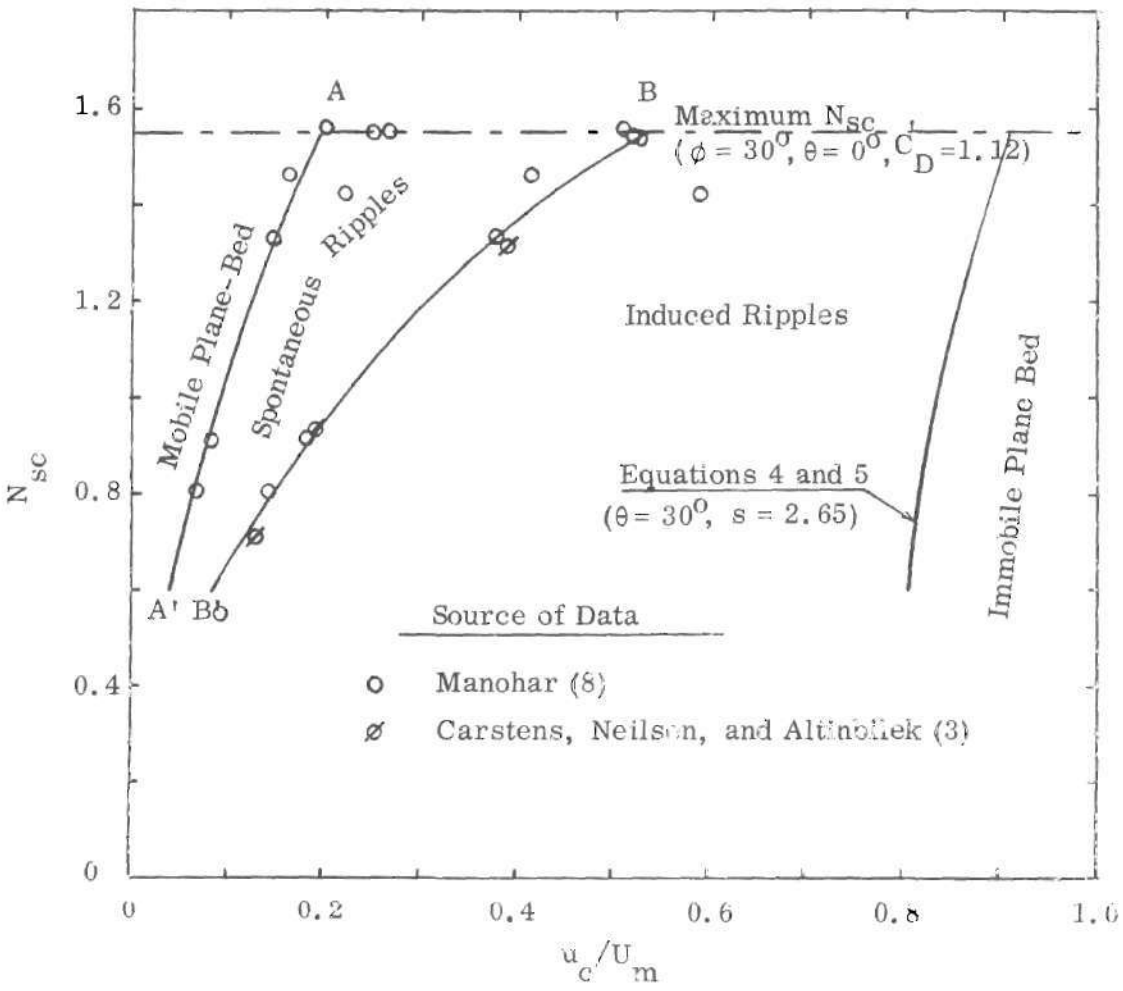

Figure 20. Transient Conditions.

water-motion velocity and is independent of the separate effects of water-motion amplitude and water-motion period. The line $\overline{AA}$ is described by the equation

$$\frac{u_c}{U_m} = \frac{N_{sc}^2}{12} \tag{34}$$

(b) The lower limit, $\overline{BB}$ in Figure 20, for the existence of spontaneous ripples has been investigated experimentally by Manohar (7) and by Carstens, Neilson, and Altinbilek (3). Manohar's data show that, for a particular bed material, this limit is a function of maximum water-motion velocity and independent of the separate effects of water-motion amplitude and water-motion period. The line $\overline{BB}$ is described by the relationship

$$\frac{u_c}{U_m} = \frac{N_{sc}^2}{4} \tag{35}$$

(c) The lower limit, $\overline{CC}$ in Figure 20, for the propagation dunes from induced ripples is computed by means of equation 5. The dunes will not propagate when the velocity at the crest of the dune is less than the threshold velocity at the crest of the dune. Since the upstream slope of a dune crest is about 30-degrees, the value, θ equal 30-degrees, is used in equation 5 to compute N_{scd}-- the smallest sediment number at which dunes will propagate. Considering equation 2, the largest value of u_c/U_m for which dunes will propagate is as follows.

$$\frac{u_c}{U_m} = 1.2 \frac{N_{sc}}{N_{scd}} \tag{36}$$

The experimental information (3) concerning the development of dunes pertains to induced ripples; that is, to initial conditions in the region between lines $\overline{BB}$ and $\overline{CC}$ in Figure 20. All of these experiments were performed with the same water-motion period -- about 3.55 seconds. The amplitude was the controlled water-motion variable and was maintained constant during a run. The information regarding the development of the bed are for two types of bed materials -- a coarse sand (D_g equal 0.585 mm, s equal 2.66) and a medium sand (D_g equal 0.297 mm, s equal 2.47). The values of N_{sc}, equation 5, for these materials are 1.31 and 0.93, respectively.

Observation (3) of the position of the dune crests during two experiments (3) are shown in Figures 21 (a and b) -- runs 48 and 54 respectively. During Run 48, which was performed with the medium sand -- N_{sc} equal 0.93, the water-motion amplitude decreased from about 0.22 feet to 0.20 feet. During Run 54, which was performed with the same medium sand, the water-motion amplitude decreased from about 0.35 feet to 0.31 feet. The locations of dune crests on the bed are shown as segmented lines in Figure 21. A dune wave length, at any time during a run, is the distance between two successive crests. As shown in Figure 21, each dune originates with an initial wave length, λ_0, and increases in size until a stable geometry is attained. The time required for the development of the dune shown in Figure 21(a), Run 48, is about 5000 cycles. The time required for the development of the dune shown in Figure 21(b), Run 54, is about 800 cycles.

Figure 22 shows the volume V_e/λ^2 eroded, during each one-half cycle of water motion, from the upstream face of a dune. In this figure, which pertains

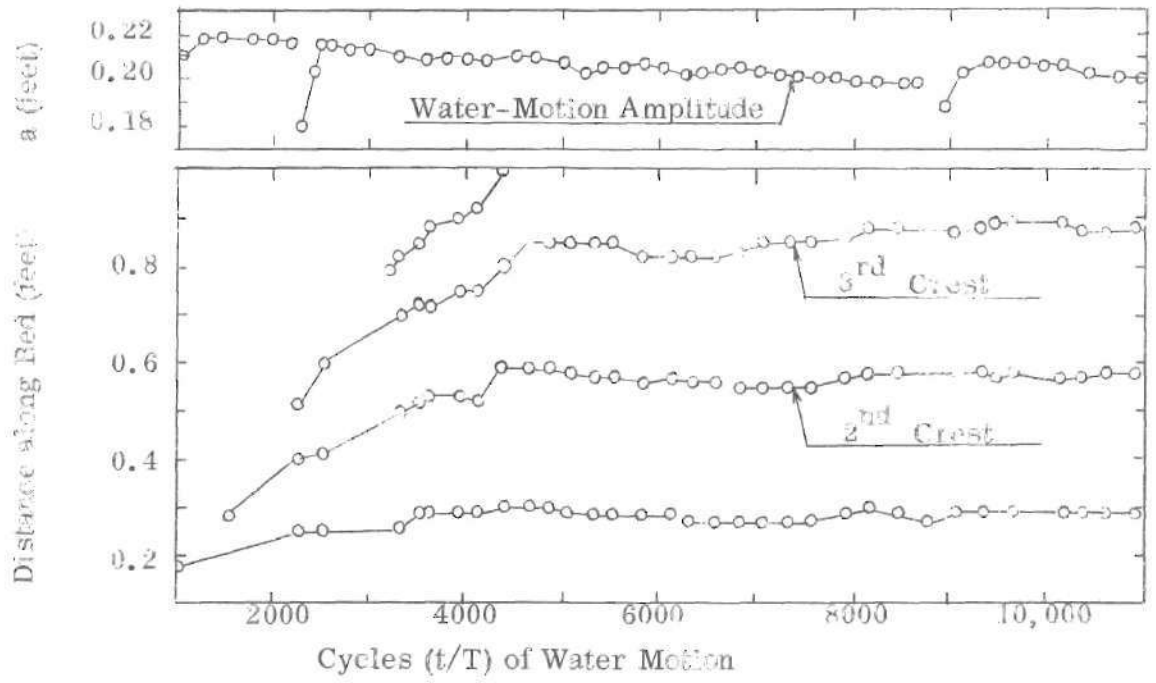

(a) Run 48 (1, 3): T = 3.55 sec, D_g = 0.297 mm, s = 2.47

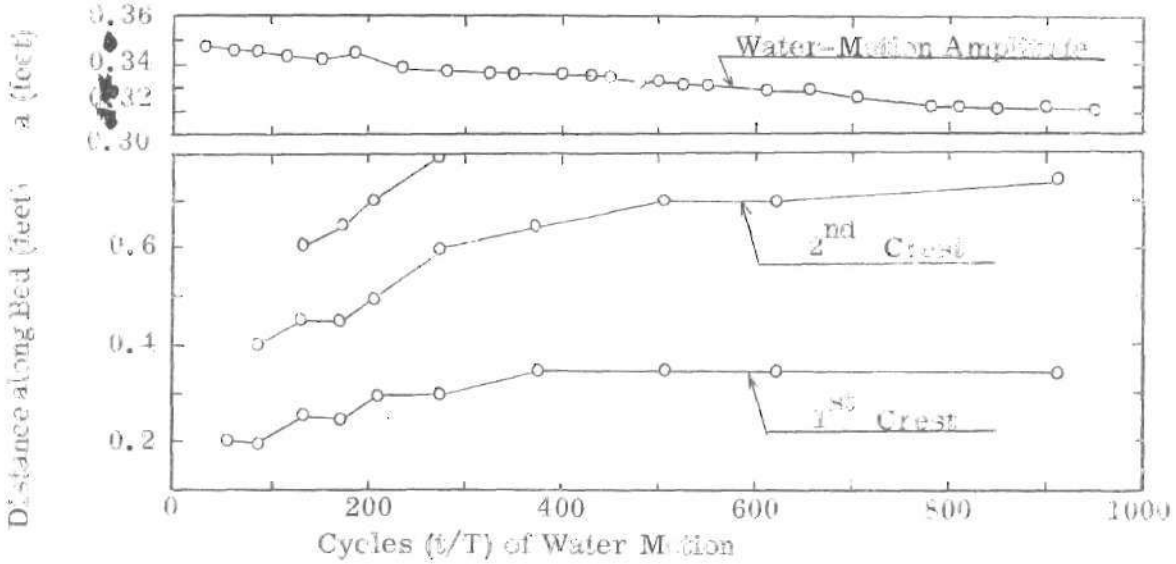

(b) Run 54 (1, 3): T = 3.68 sec., D_g = 0.297 mm, s = 2.47

Figure 21. Development of a Duned Bed From Induced Ripples.

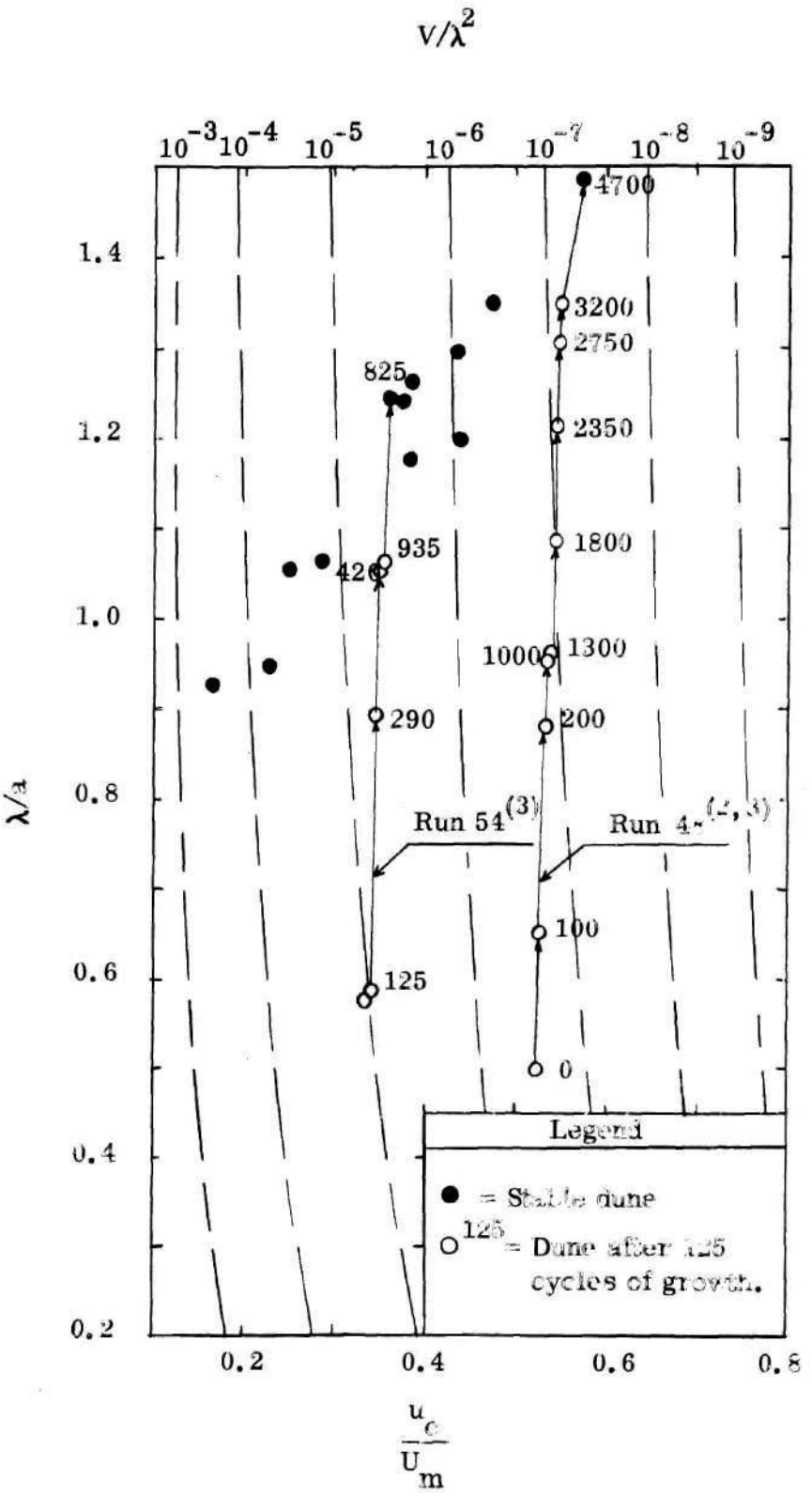

Figure 22. Development of a Duned Bed (N_{sc} = 0.93).

to a particular N_{sc}, the values of V_e/λ^2 are expressed in terms of two parameters -- λ/a and u_c/U_m. In Figure 22 the value of N_{sc}, 0.93, is that of the medium sand (3). The growing dunes, previously shown in Figures 21 (a and b), are shown in Figure 22 as dashed lines. Times, expressed in cycles after the first observation of the forming crest, are listed, in Figure 22, adjacent to selected points during the development of these two dunes. Data (3), for equilibrium dunes of medium sand, from ten other runs are also depicted in Figure 22.

The experimental data (3) shown in Figure 22 provide information regarding the development of dunes on an initially plane bed as the bed is subjected to oscillatory water motion. Recalling that Figure 22 pertains to a bed material having a specific N_{sc}, 0.93, and that during each of the depicted runs, Run 48 and Run 54, the maximum water-motion velocity was maintained essentially constant, the following information regarding development of dunes is shown in Figure 22.

(a) The dunes develop more rapidly at low values, Run 54, of u_c/U_m than at high values, Run 48, of u_c/U_m. That is, although the times at which the dunes become stable are not precisely shown in either Figure 21 or Figure 22, the approximate time for a dune to develop to equilibrium is only about 825 cycles during Run 54 whereas it is about 4700 cycles during Run 48 as shown in Figure 22. The dimensionless volume, V_e/λ^2 decreases during the run. The experimental information, as shown in Figure 21, shows that the wave length λ increases from an initial value λ_o to an equilibrium value. Consequently the actual volume V_e eroded per one-half cycle per dune remains essentially constant during the development. A constant V_e during development precludes its being the factor, per se, which

causes the dune to be in equilibrium. In addition, the steepness of the curves V_e/λ^2 equal constant as shown in Figure 22 indicate a relatively insensitive relationship between λ/a and V_e/λ^2 during the development and at equilibrium.

Figure 23 is a diagram, similar to Figure 22, showing observations (3) of stable dunes on a coarse sand. The value of N_{sc} of this coarse sand, is 1.31 which is also the value of N_{sc} used in establishing the values of V_e/λ^2 in Figure 23. As shown in Figure 23, there is considerable scatter in the observed values of λ/a at equilibrium -- particularly at low values of u_c/U_m.

C. Types of Equilibrium Dunes

The development of the bed will cease whenever the volume of bed material removed from the upstream face of a dune during one-half cycle of water motion equals the volume of material deposited along the same face during the following one-half cycle. In other words, a dune will not enlarge if the net volume of material removed from or deposited on the crest is zero during each cycle of water motion.

Profiles of an eroding dune have been shown previously in Figure 10. The elevation of the crest of an equilibrium dune is the same at the beginning and at the end of each half cycle; that is, y_{c1} equal y_{c2} in Figure 10. In addition, the elevation, y_a in Figure 10, at the least value of x at which erosion occurs and the elevation, y_d in Figure 10, of the toe of the fill are the same. Assuming that the upstream face of the dune is plane and inclined at the angle θ between the location x_a, in Figure 10, and the crest then geometrical considerations require that, for an equilibrium dune,

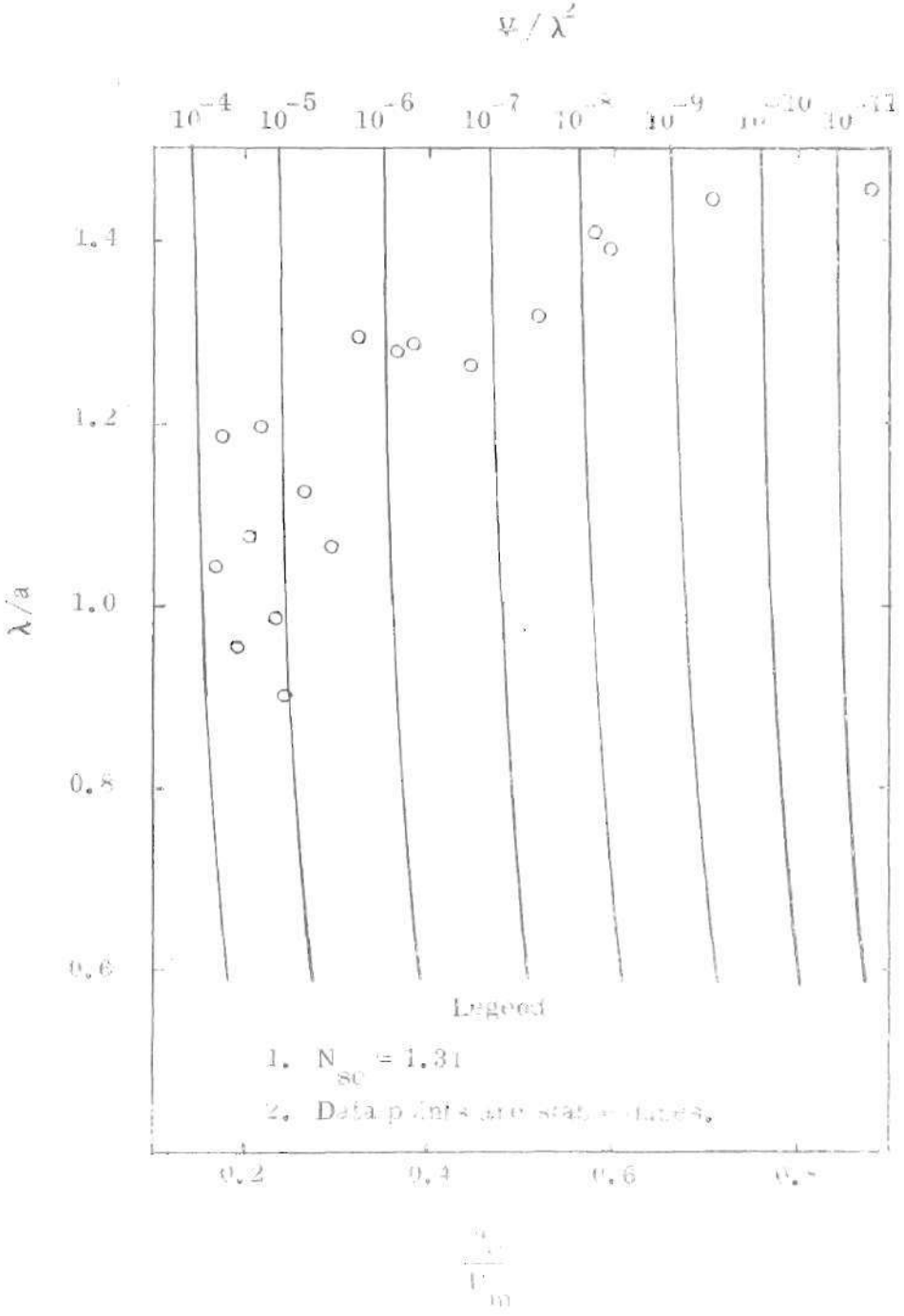

Figure 23. Equilibrium Dunes (Curve Set).

$$\tan \theta = \frac{\eta/\lambda_s - y_a/\lambda_s}{0.5 - \frac{x_a}{\lambda_s} - \frac{\delta_c}{2\lambda_s}} \tag{37}$$

in which λ_s is the wave length of the stable (equilibrium) dune . Experimental observations (3), such as shown previously in Figure 3, indicate that an average value of η/λ is about 0.18 for an equilibrium dune. Therefore, using η/λ equal 0.18 and letting an arc of a circle approximate the profile of the dune, elevations along the upstream face between x equal zero and x equal x_a are

$$\frac{y}{\lambda_s} = 0.7844 - \left| \sqrt{0.6153 - \left(\frac{x}{\lambda_s}\right)^2} \right| \tag{38}$$

The value of x_a/λ_s is a known function, equation 4 with t/T equal zero, of u_c/U_m. Combining equation 4, 33, 37, and 38 and solving for the stable dune wave-length λ_s,

$$\lambda_s = \frac{a N_{sc}^4 \; f_3\left(\frac{u_c}{U_m}\right)}{\sin\theta\left(1.0 - \frac{u_c}{1.2\,U_m}\right) + \cos\theta\left(\left|\sqrt{2.4612 - \left(\frac{u_c}{1.2\,U_m}\right)^2}\right| - 1.2088\right)} \tag{39}$$

In equation 39 the values of $f_3\,(u_c/U_m)$ are those shown previously in Figure 19.

Equation 39 describes the stable-dune wave length in terms of bed-material properties and water-motion characteristics provided the angle, θ, is known. The shape of the downstream face of the region of fill is a consequence of deposition

of the sediment that passes the crest and is carried into the lee vortex. This complex phenomena is not described by the analysis. However, the photographs, Figure 4, indicate that the assumption of a linear shape, or a constant θ, is not unreasonable. Physical considerations require that the inclination of the downstream slope of the region of fill does not greatly exceed the angle of repose Φ of the bed material. In other words, θ may exceed Φ, to a value Φ_d, only because the upstream velocity, along the downstream face of the fill, creates a stabilizing (drag) force on the surface particles along the face. Consequently, although the precise value of θ is not known, there is an approximate range of values, $\tan^{-1}[2\eta/\lambda] < \theta < \Phi_d$, within which θ must exist.

Additional insight into the nature of dunes is obtained by considering the relative effects of x_a/λ_s and $\delta_c/2\lambda_s$ in equation 37. The least value of x at which erosion occurs, x_a/λ_s, is a linear function, equation 4, of u_c/U_m. For a particular value of $\lambda_s \sin\theta/aN_{sc}^4$ the value of $\delta_c/2\lambda_s$ is much more sensitive to u_c/U_m as shown in Figure 19. Thus two conditions, $x_a/\lambda_s \gg \delta_c/2\lambda_s$ and $x_a/\lambda_s \ll \delta_c/2\lambda_s$, dominate equation 37. The first condition is simply that the movement of the crest is extremely small. In this situation, using equation 4 and 38, equation 37 may be evaluated as follows.

$$\theta = \tan^{-1}\left(\frac{\left|\sqrt{2.4612 - \left(\frac{u_c}{1.2\,U_m}\right)^2}\right| - 1.2088}{1.0 - \frac{u_c}{1.2\,U_m}}\right) \qquad (40)$$

The second condition states that the movement of the crest is large in comparison

with the value of x_a/λ_s. In this situation, using equations 4, 33, and 38, equation 37 may be evaluated in the form

$$\frac{\lambda_s}{a N_{sc}^4} = \frac{f_3\left(\frac{u_c}{U_m}\right)}{\sin\theta - \cos\theta \left(\left| \sqrt{2.4612 - \left(\frac{u_c}{1.2U_m}\right)^2} \right| - 1.2088 \right)} \quad (41)$$

As indicated in Figure 19, equation 40 pertains to larger values of u_c/U_m whereas equation 41 pertains to low values of u_c/U_m. Figure 24 shows values of λ_s/aN_{sc}^4 as a function of u_c/U_m, for different values of θ, as evaluated by means of equations 40 and 41.

Observers (1, 3) have noted that dunes may be three-dimensional, transitional, or two-dimensional. The physical conditions which cause these three types of dunes are the following:

(a) Three-dimensional dunes, considering a particular bed material, occur (1, 3) at high maximum water-motion velocities; that is, at low values of u_c/U_m. An obvious situation which causes the profile of a dune system to be irregular occurs whenever the angle θ, equation 37, is significantly greater than the angle of repose of the bed material. In other words, the geometrical conditions (equation 37) required for a periodic recurrence of each dune profile are not physically possible.

(b) Transitional dunes, considering a particular bed material, occur (1, 3) at intermediate maximum water-motion velocities. The profiles of these dunes are quite regular whereas, in plan, the crests are irregular and may be broken.

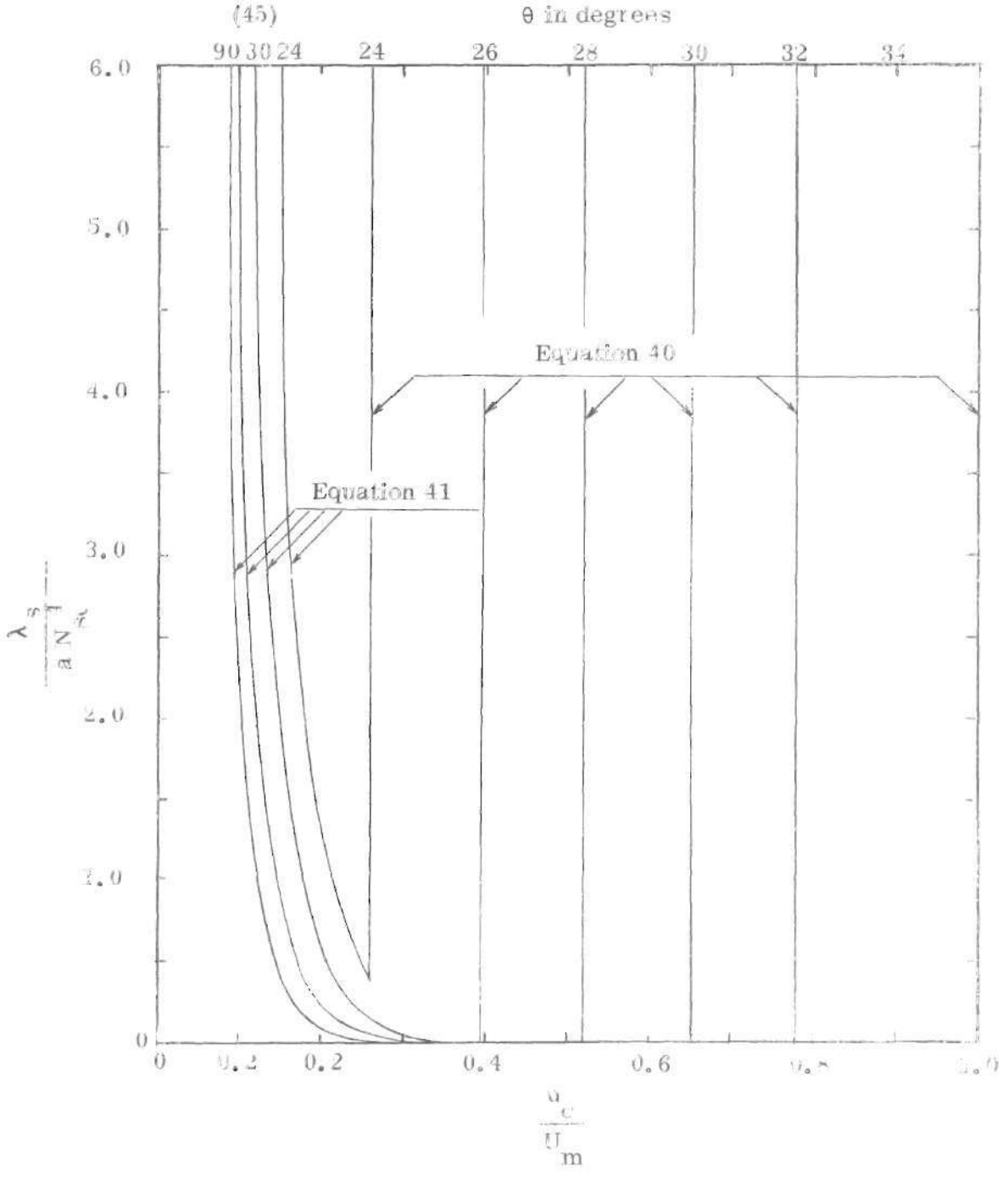

Figure 24. Approximate Geometrical Requirements for a Settle Duct.

A large irregular movement of any section of a dune crest will subsequently cause an irregular movement, due to erosion, of the adjacent crests. Consequently, although geometrical conditions, equation 37, required for a stable dune profile are satisfied, a plan view of the bed is expected to show irregularities in the dune crests.

(c) Two-dimensional dunes occur (1, 3) at low maximum water-motion velocities. In order for the profile of these dunes to reoccur each cycle the geometrical condition, equation 37, must be satisfied. In addition the erosion, and movement, of the crest of each dune must be small so that irregularities, in plan, of any section of the crest do not influence the erosion of adjacent crests.

The delineation, in terms of the parameters previously shown in Figure 24, of these three types of bed configurations are shown in Figure 25. The value θ equal 45^{o} is chosen to delineate three-dimensional dunes from the transition region. The transition region is separated from the region of two-dimensional dunes by a line passing through the intersection of the curves, θ equal constant, defined by equation 42 and the value of u_c/U_m, for a corresponding θ, defined by equation 41. Of course at extremely low values of u_c/U_m a mobile plane bed, as shown in Figure 20, occurs. At high values of u_c/U_m dunes will not propagate and an immobile plane bed, as shown in Figure 20 occurs.

Experimental data (3), shown in Figure 25, provide known information regarding equilibrium configurations of a duned bed. The plotted data (3) pertain to the coarse and medium sands previously described and to a fine sand (D_g equal 0.190 mm, s equal 2.62, and N_{sc} equal 0.71). The delineation of the data according

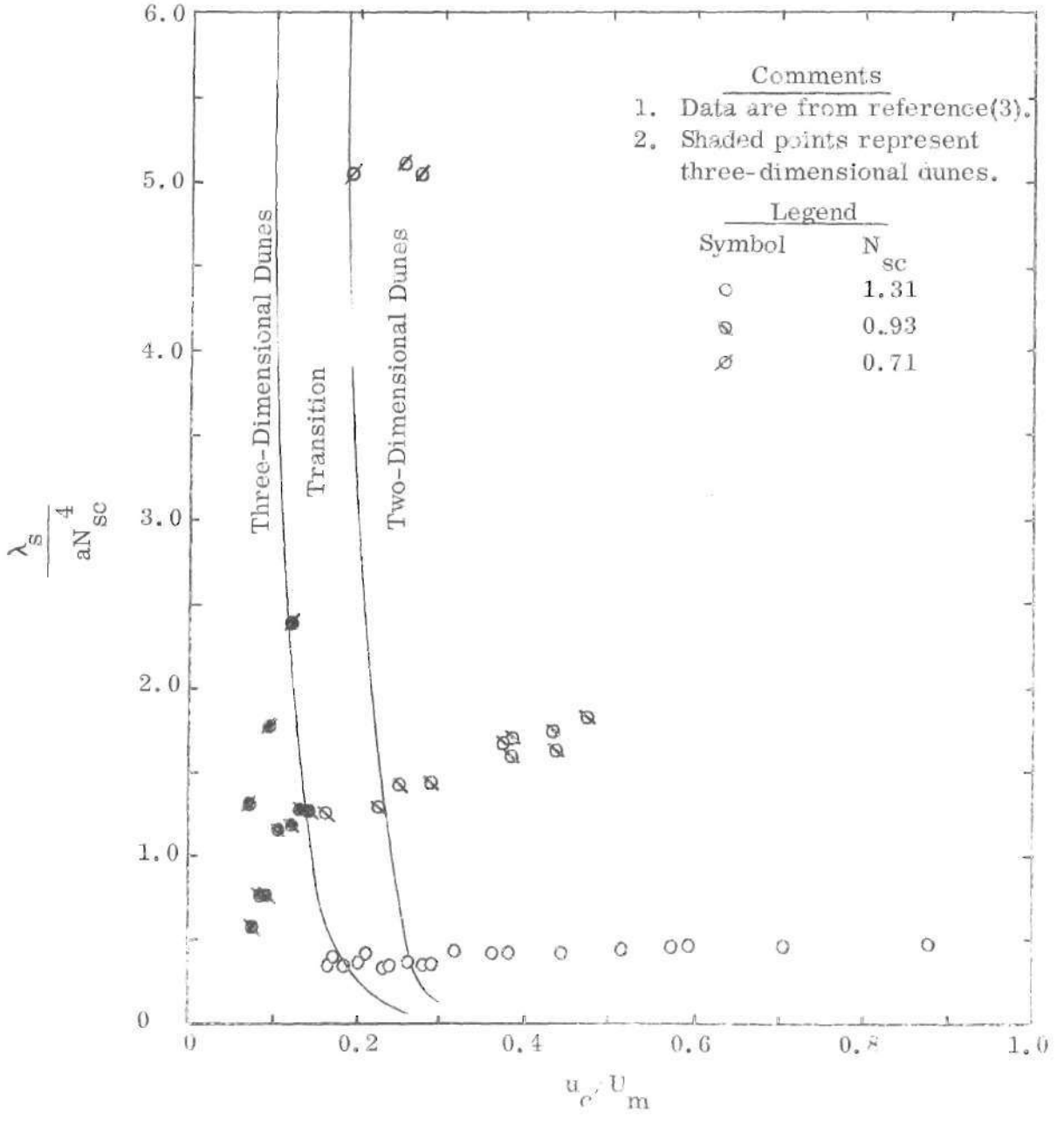

Figure 25. Dune Types.

to the analytical concepts agrees with the observed occurrence of three-dimensional dunes. No precise information regarding the transition region is available. However, it is known (3) that this region extends over a range of values of u_c/U_m as indicated in the analysis, Figures 24 and 25.

D. Equilibrium Dune Geometry

As shown in Figure 25, two-dimensional dunes occur at higher values of u_c/U_m. Only a small amount of erosion occurs along a stable two-dimensional dune. Equilibrium conditions are dependent on the location of x_a; that is two-dimensional dunes exist in the region, Figure 25, in which the movement of the crest is small and sediment fills a distance, along the downstream face, a distance $\lambda/2 - x_a$. The water-motion in the lee-vortex is complex and is not amenable to analysis, however, the previous analysis, equation 40, shows that a unique relationship exists between the slope of the downstream face and the parameter u_c/U_m. Assuming a linear relationship between the water-motion amplitude and the extension of the fill

$$\frac{a}{\lambda_s} = \frac{1}{2C} - \frac{1}{2.4C}\left(\frac{u_c}{U_m}\right) \tag{42}$$

in C is an assumed constant.

The experimental data (3) are shown in Figure 26 using the above relationship. The data indicate that

$$\frac{a}{\lambda_s} \approx 0.8 - \frac{2}{3}\left(\frac{u_c}{U_m}\right) \tag{43}$$

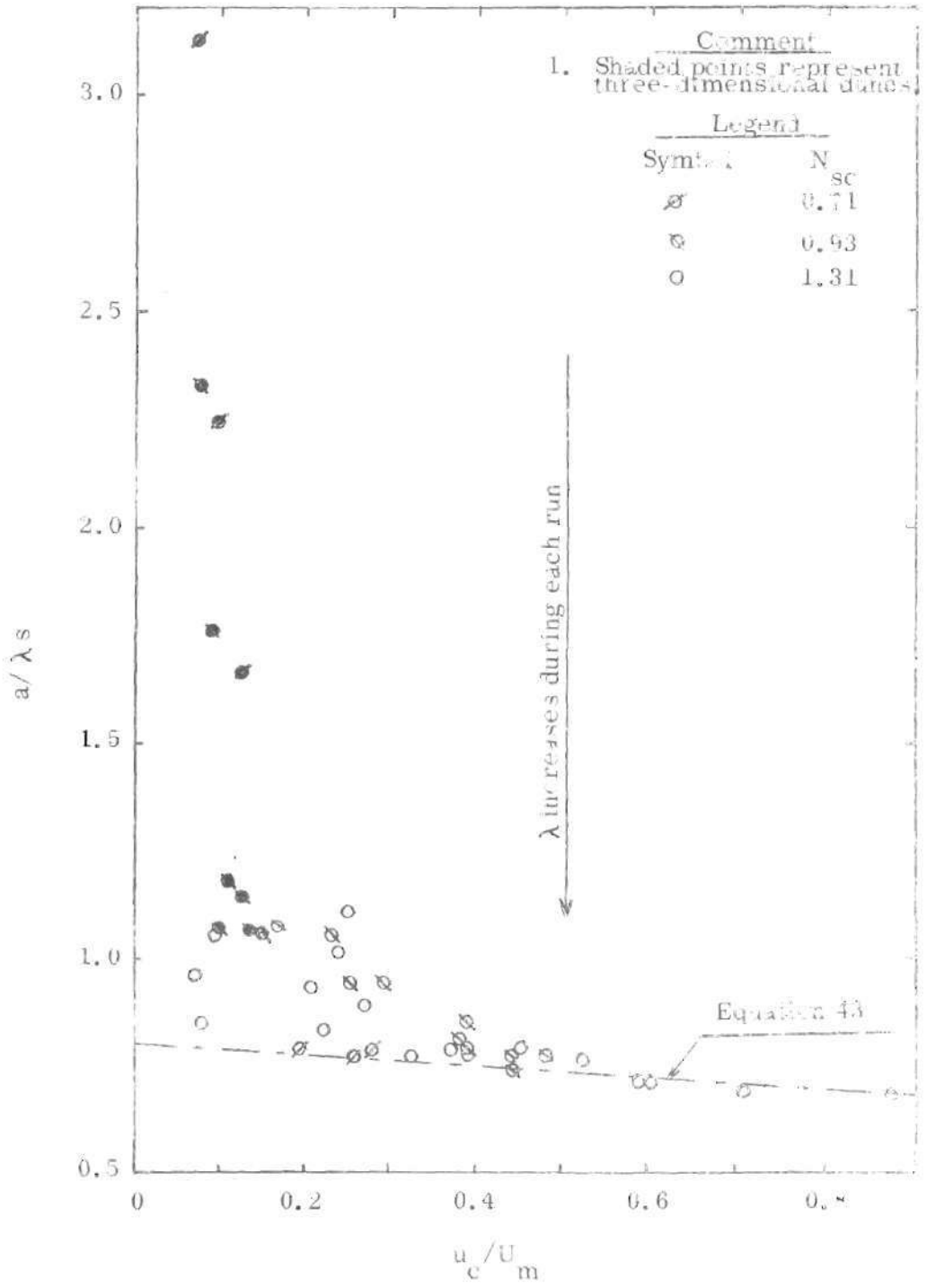

Figure 26. Wave Lengths of Stable Dunes (3).

that is, C equal 0.625.

The part of the data (3), shown in Figure 26, regarding the two-dimensional dunes pertains to geometrically similar dune profiles, Table 1. That is, the ratio of dune height to dune wave length, η/λ, has a value of about 0.18 regardless of sand size. Other investigators (4, 5, 6, 7, 8) have shown a range in values, extending down to a near zero value, of η/λ. The reason for these low values of η/λ not known. The results of three authors (4, 5, 6) are shown in Figure 27(a). These data indicate that, for η/λ near zero, the value of C, equation 42, is 1.35.

The data of Inman (6) is shown in a similar manner in Figure 27 (b). The major portion of his observations, after differentiating between two- and three-dimensional features, fall in the region between C equal 0.625 and C equal 1.35. The scatter in his data can readily be attributed to the uncontrolled factors inherent in data obtained in the field. In particular, information regarding the initial bed configuration and information regarding time for development are not available.

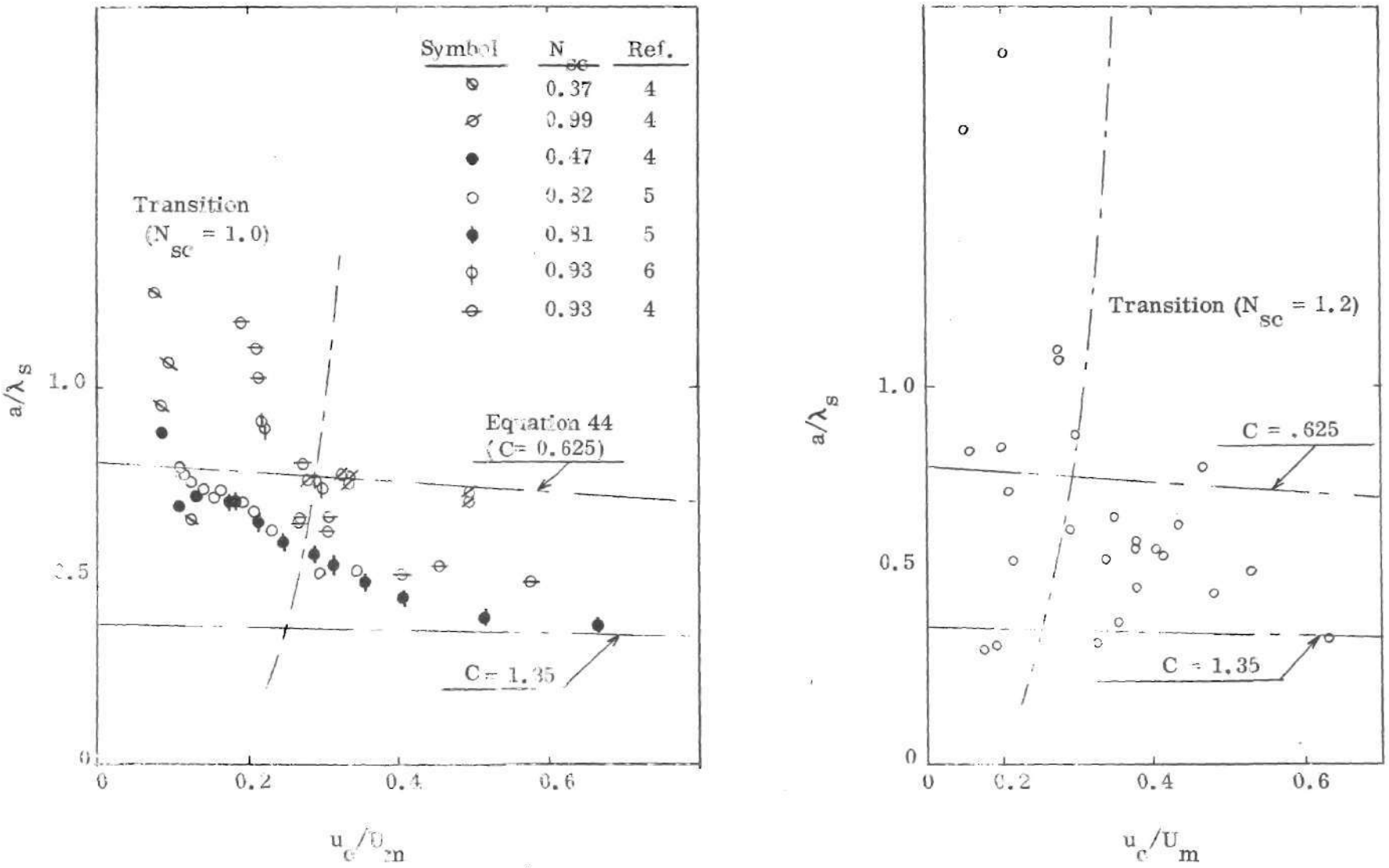

(a) Laboratory Investigations

(b) In Situ Measurements (7)

Figure 27. Stable Dune Wave Lengths (4, 5, 6, 7).

CHAPTER V

CONCLUSIONS

The behavior of a sediment-water interface under oscillatory flow is a complex phenomena. The characteristics of the bed forms are dependent on sediment and fluid properties and on the characteristics of the water motion. In addition, since changes in the bed forms are brought about by localized scour and fill along the bed surface, the characteristics of the bed forms are dependent on the initial conditions (bed forms) and on the time allowed for the development of the bed.

The theory considers space and time variations in erosion and deposition along the bed and, therefore, describes the mechanism by which the characteristics of the bed forms change. The analysis considers the particular situation in which an initially plane bed is subjected to oscillatory water motion. This model situation is not the general case in nature nor is it always used in laboratory investigations. In particular, the situation in which small amplitude water-motion is introduced over relatively long amplitude bed forms has been observed (2, 8). This latter situation, a/λ_o equalling about one-sixth (2), leads to the formation of 'brick-pattern' dunes which have not been considered herein. The theory does show that for lower values of a/λ the deposition along the upstream face becomes significant with respect to the total volume eroded from the upstream face. This increased deposition is probably a key factor governing the stability of brick

pattern dunes.

The analysis allows the characteristics of the bed forms, developing along the interface of a plane sediment bed subjected to oscillatory water motion, to be predicted as follows.

A. Transient Conditions

If either an immobile or mobile plane bed exist, according to Figure 19 (or equations 34 and 36), the plane-bed will not deform. However, if either spontaneous ripples or induced ripples exist, according to Figure 19, the plane-bed will deform.

B. Stable Dunes

The stable dune wave length is evaluated by means of equation 48; that is

$$\lambda_s = \frac{a}{0.8 - \frac{2u_c}{3U_m}}$$

The shape and type of stable dune is determined by means of Figure 25 (or equations 41 and 42) -- if the stable dune is three-dimensional then neither the value of λ_s obtained by means of equation 48 nor the value of η/λ_s, 0.18, are applicable.

C. Development of the Bed

The time required for, and the rate of, development of the bed are not analyzed. Only an insight into the rate of development is obtained when the net volume eroded from the upstream during one-half cycle of water motion is

evaluated -- equation 28 and Figure 14(b). In other words the net volume eroded from the upstream face cannot be extrapolated into a volumetric growth of the dune crest per half cycle inasmuch as erosion also occurs along the downstream face of the growing dune.

Three significant points regarding the removal of sediment from the upstream face are revealed by the theory. Firstly, the erosion along a dune face occurs, for the most part, near the crest, x equal $\lambda/2$, of the dune as shown in Figure 17. Secondly, the time lag between the time of maximum rate of sediment transport and maximum water-motion velocity is generally small as shown in Figure 16. Finally the amount of material deposited along the upstream face of a dune is generally insignificant when compared to the amount of material eroded from the upstream face during the same half cycle of water motion, as shown in Figure 14.

CHAPTER VI

RECOMMENDATIONS

Erosion and deposition of sediment are of practical importance in the evaluation of localized scour, hydraulic roughness, and bed-load sediment transport in both uni-directional and oscillatory fluid motion over an erodible bed. However fundamental equations defining the pickup and deposition of sediment as functions of the bed-material and fluid properties, and the fluid motion characteristics are not known. It is therefore recommended that analytical and experimental research be directed towards the determination of these fundamental equations.

Two phenomena, regarding investigations concerning oscillatory flow over a duned bed, should be studied. Firstly an analysis of erosion and deposition along the downstream face of the dune, for the primary purpose of evaluating the rate of development of the bed, is in order. Secondly, an investigation of the consequences of having a deformed bed as an initial condition should be studied.

APPENDIX A

EROSION ALONG THE UPSTREAM FACE

Manipulation of the sediment pickup function, equation 11, is cumbersome and therefore evaluations presented in the text, section II. G, were obtained by summation processes. The total forward movement, δ_e, due to erosion at location x_r and for the total volume V_e eroded from the upstream face are approached herein through integration of equations 12 and 21a respectively. The advantage of the numerical approach presented previously is obvious.

A. Total Forward Movement Due to Erosion

The total forward movement, δ_e, due to erosion at location x_r during one-half cycle is described by equation 12. Assuming there is no change in slope, θ, at location x_r during the one-half cycle and using equations 4 and 11, equation 12 may be expressed as

$$\left(\frac{x_a}{x_r}\right)^5 \frac{\sin\theta}{10^{-4}(u_c/U_m)N_{sc}^4} \quad \frac{\delta_e}{a} = \int_{t_{r1}}^{t_{r2}} \cos^5 t \left[1-\left(\frac{x_a}{x_r}\right)^2 \cos^{-2} t\right]^{10} dt \quad (44)$$

in which t, t_{r1} and t_{r2} are expressed in radians. As before x_a is equal to $u_c\lambda/2.4\,U_m$, t_{r1} is equal to $-t_{r2}$, and t_{r2}, $0 \le t_{r2} \le \pi/2$, is equal to $\cos^{-1}(u_c\lambda/2.4\,U_m\,x_r)$. For convenience equation 44 is expressed as

$$\delta_e = 2A \int_0^{t_{r2}} \cos^5 t \left(1 - \left(\frac{x_a}{x_r}\right)^2 \cos^{-2} t\right)^{10} dt \qquad (45)$$

in which A is equal to $\dfrac{aN_{sc}{}^4 u_c 10^{-4} x_r^5}{5 U_m x_a \sin\theta}$ from equation 44.

The integrand in equation 45 may be expanded by means of the binomial theorem* and evaluated** in the form

$$\delta_e = 2A \sum_{i=0}^{10} \frac{(-1)^i 10!}{(10-i)!\,i!} \left(\frac{x_a}{x_r}\right)^{2i} \int_0^{t_{r2}} \cos^{5-2i} t \; dt \qquad (46)$$

Six of the eleven terms comprising equation 46 are shown in Table A1. Also given in Table A1, is a recursion formula by which the remaining terms may be evaluated.

B. Total Erosion Along the Upstream Face

The total erosion, V_e, along the upstream face is described by equation 21a. Letting θ equal constant along the upstream face, equations 46 and 21a show

- - - - - - -

*For example, reference (11), page 97, equation 814.

**Op cit, pages 41-42, equations 274 and 284.

that

$$\frac{V_e}{\tan\theta} = \int_{x_a}^{\lambda/2} \left(2A \sum_{i=0}^{10} \frac{(-1)^i 10!}{(10-i)!\,i!} \left(\frac{x_a}{x_r}\right)^{2i} \int_0^{t_{r2}} \cos^{5-2i}(t)\,dt \right) dx_r \qquad (47)$$

In equation 47 the parameters A and t_{r2} are functions of the variable x_r. In view of the complex expressions, Table A1, describing each term in the integrand of equation 47, the advantage of using a summation procedure, such as the procedure used in the text, is obvious.

Table A1. Analytical Expression For Forward Movement, δ_e, During One-Half Cycle

Term	Coefficient	Integral
i	$\frac{2A(-1)^i 10!}{(10-i)!\,i!}\left(\frac{x_a}{x_r}\right)^{2i}$	$\int_a^{t_{r2}} \cos^{5-2i}(t)\,dt$
0	$2A$	$\frac{\cos^4(t_{r2})\sin(t_{r2})}{5} + \frac{4\cos^2(t_{r2})\sin(t_{r2})}{15} + \frac{8\sin(t_{r2})}{15}$
1	$-20A\left(\frac{x_a}{x_r}\right)^2$	$\frac{\sin(t_{r2})\cos^2(t_{r2})}{3} + \frac{2\sin(t_{r2})}{3}$
2	$90A\left(\frac{x_a}{x_r}\right)^4$	$\sin(t_{r2})$
3	$-240A\left(\frac{x_a}{x_r}\right)^6$	$\ln\tan\left(\frac{t_{r2}}{2} + \frac{\pi}{4}\right)$
4	$420A\left(\frac{x_a}{x_r}\right)^8$	$\frac{\sin(t_{r2})}{2\cos^2(t_{r2})} + \frac{\ln\tan\left(\frac{t_{r2}}{2}+\frac{\pi}{4}\right)}{2}$
5	$-504A\left(\frac{x_a}{x_r}\right)^{10}$	$\frac{\sin(t_{r2})}{4\cos^4(t_{r2})} + \frac{3\sin(t_{r2})}{8\cos^2(t_{r2})} + \frac{3\ln\tan\left(\frac{t_{r2}}{2}+\frac{\pi}{4}\right)}{8}$
6-10	$\frac{2A(-1)^i 10!}{(10-i)!\,i!}\left(\frac{x_a}{x_r}\right)^{2i}$	$\frac{\sin(t_{r2})}{(2i-6)\cos^{2i-6}(t_{r2})} + \frac{2i-7}{2i-6}\int_0^{t_{r2}} \frac{dt}{\cos^{2i-7}(t)}$

APPENDIX B

DUNE GEOMETRY

Table 1. Dune Geometry -- R. A. Bagnold (2)

D_g (mm)	s	N_{sc}	λ/a	a/D_g
0.090	2.65	0.35	0.181	3556
			0.305	2111
			4.462	1444
			0.864	733
			1.205	433
			1.685	211
			1.678	166
			2.014	80
0.160	2.65	0.60	0.253	2000
			1.194	419
			2.001	119
0.360	2.65	1.04	0.391	889
			0.658	528
			0.839	414
			0.962	361
			1.333	250
			1.424	183
			1.713	78
			1.976	49
0.800	2.65	1.47	0.563	400
			0.740	313
			0.947	238
			1.242	186
			1.385	163
			1.924	115
			1.848	83
			1.742	49
0.360	1.30	0.74	0.579	528
			1.133	250
			1.243	183
			1.668	108

Table 1 (Concluded). Dune Geometry -- R. A. Bagnold (2)

D_g (mm)	s	N_{sc}	λ/a	a/D_g
			1.925	75
			2.216	51
2.500	1.30	1.64	0.641	128
			1.079	76
			1.538	52
			1.758	36
			1.716	27
			1.500	18
0.360	7.90	1.30	0.328	889
			0.553	528
			0.754	361
			0.902	256
			1.061	183
			1.359	108
			1.879	41
0.600	7.90	1.52	0.947	317
			1.077	217

Table 2. Dune Geometry -- Carstens, Neilson, and Altinbilek (3)

D_g (mm)	s	N_{sc}	η/a	λ/a	η/λ	N_{sm}	$T\sqrt{\frac{(s-1)g}{D_g}}$	$\frac{a}{D_g}$
0.190	2.62	0.71	0.232	1.287	0.180	2.82	1056	474
			0.206	1.278	0.161	3.74	1048	625
			0.081	0.599	0.134	4.79	1036	956
			0.056	0.446	0.126	7.58	1033	1247
			0.015	0.320	0.047	10.02	1033	1649
			0.253	1.274	0.199	2.60	1039	430
0.297	2.47	0.93	0.201	1.178	0.171	2.43	785	304
			0.185	1.062	0.175	3.23	785	403
			0.185	1.056	0.175	3.72	782	463
			0.170	0.949	0.179	4.12	782	513
			0.158	0.930	0.170	5.64	782	702
			0.153	0.947	0.162	6.32	782	787
			0.124	0.940	0.132	7.09	778	878
			0.097	0.847	0.115	8.66	780	1075
			0.060	0.568	0.106	9.64	776	1191
			0.011	0.428	0.026	12.16	776	1501
			0.037	0.567	0.065	10.53	782	1304
			0.115	0.876	0.131	7.57	782	942
			0.238	1.297	0.183	2.15	789	269
			0.198	1.261	0.157	2.42	756	291
			0.210	1.198	0.175	2.13	730	248
			0.217	1.240	0.175	2.48	811	321
			0.229	1.349	0.170	1.97	835	261
0.585	2.66	1.31	0.275	1.453	0.189	1.49	585	139
			0.275	1.445	0.190	1.85	588	173
			0.272	1.390	0.195	2.20	586	205
			0.244	1.315	0.186	2.53	584	235
			0.245	1.265	0.193	2.94	586	275
			0.245	1.287	0.190	3.41	584	317
			0.264	1.280	0.206	3.59	588	336
			0.260	1.298	0.200	4.09	586	382
			0.197	1.063	0.185	4.45	584	414
			0.197	1.066	0.185	4.57	582	423
			0.210	1.125	0.187	4.91	582	455
			0.173	0.901	0.192	5.34	585	497
			0.194	0.987	0.197	5.64	587	526
			0.180	1.197	0.150	5.99	586	559
			0.194	1.075	0.181	6.49	582	601
			0.165	0.955	0.173	6.88	584	640
			0.175	1.182	0.148	7.35	573	670
			0.164	1.041	0.157	7.76	586	724
			0.254	1.408	0.180	2.26	587	211

Table 3. Dune Geometry -- Kennedy and Falcon (4)

D_d (mm)	s	N_{sc}	η/a	λ/a	η/λ	N_{sm}	$T\sqrt{\frac{(s-1)g}{D_g}}$	a/D_g
0.095	2.67	0.37	0.257	1.539	0.167	2.95	444	209
			0.138	0.800	0.173	4.85	810	626
			0.209	1.057	0.197	4.36	810	561
			0.171	0.942	0.182	3.94	972	610
			0.023	0.181	0.126	6.40	3040	3096
			0.026	0.218	0.118	5.04	3040	2438
			0.066	0.312	0.213	10.56	1603	2695
0.320	2.67	0.99	0.214	1.300	0.165	3.04	315	152
			0.219	1.354	0.162	2.95	355	167
			0.254	1.338	0.190	3.54	355	200
			0.247	1.310	0.189	2.95	315	148
			0.297	1.393	0.213	2.36	355	133
			0.222	1.438	0.154	2.00	315	100
1.000	1.04	0.93	0.000	0.000*******		4.54	34	24
			0.035	0.857	0.041	4.83	34	26
			0.000	0.000*******		1.41	34	8
			0.000	0.000*******		3.11	34	17
			0.077	1.257	0.061	3.39	34	18
			0.076	1.525	0.050	3.04	41	20
			0.079	1.559	0.050	3.51	41	23
			0.000	2.075	0.000	1.61	42	11
			0.178	1.987	0.089	2.31	42	15
			0.000	0.000*******		2.77	42	18
			0.231	1.534	0.151	3.47	52	29
			0.250	2.197	0.114	1.76	54	15
			0.000	0.000*******		4.75	34	26
			0.000	0.000*******		6.98	34	38
			0.049	0.908	0.054	4.40	44	31
			0.212	1.625	0.131	3.07	53	26
			0.101	0.975	0.104	4.34	53	37
0.107	1.35	0.47	0.000	1.415	0.000	3.60	199	114
			0.220	1.146	0.192	5.34	335	285
			0.255	1.471	0.174	4.31	353	242
			0.000	0.000*******		5.22	428	356
			0.000	0.000*******		4.06	529	342
			0.000	0.000*******		4.54	276	199

Table 4. Dune Geometry -- Yalin and Russell (5)

D_g (mm)	s	N_{sc}	η/a	λ/a	η/λ	N_{sm}	$T\sqrt{\frac{(s-1)_g}{D_g}}$	a/D_g
0.480	1.19	0.82	0.454	1.944	0.233	2.39	113	43
			0.377	1.954	0.193	2.76	113	50
			0.262	1.611	0.163	3.51	113	63
			0.235	1.501	0.157	3.91	113	71
			0.203	1.440	0.141	4.23	113	76
			0.161	1.372	0.117	4.92	113	89
			0.130	1.409	0.092	5.35	113	97
			0.121	1.382	0.087	5.73	113	104
			0.099	1.366	0.072	5.84	113	105
			0.073	1.368	0.053	6.31	113	114
			0.062	1.334	0.046	6.56	113	118
			0.033	1.305	0.025	7.00	113	126
			0.016	1.283	0.012	7.39	113	133
0.355	1.48	0.81	0.631	2.748	0.230	1.21	115	22
			0.580	2.587	0.224	1.57	115	29
			0.534	2.260	0.236	1.99	115	37
			0.469	2.083	0.225	2.29	115	42
			0.409	1.886	0.217	2.58	115	47
			0.376	1.784	0.211	2.80	115	51
			0.284	1.697	0.167	3.25	115	60
			0.243	1.558	0.156	3.77	115	69
			0.193	1.430	0.135	4.38	115	80
			0.190	1.434	0.132	4.45	115	82
			0.182	1.436	0.127	4.58	115	84

Table 5. Dune Geometry -- Inman and Bowen (6)

D_g (mm)	s	N_{sc}	η/a	λ/a	η/λ	N_{sm}	$T\sqrt{\frac{(s-1)g}{D_g}}$	a/D_g
0.290	2.65	0.93	0.224	1.326	0.169	3.21	331	169
			0.213	1.382	0.154	3.08	331	162
			0.208	1.354	0.154	3.14	331	166
			0.208	1.334	0.156	3.14	331	166
			0.156	1.125	0.139	4.40	473	331
			0.173	1.103	0.157	4.24	473	319
			0.161	1.140	0.141	4.26	473	321
			0.176	1.132	0.155	4.17	473	314

Table 6. Dune Geometry -- Douglas L. Inman (7)

D_g (mm)	s	N_{sc}	η/a	λ/a	η/λ	N_{sm}	$T\sqrt{\frac{(s-1)g}{D_g}}$	a/D_g
0.118	2.65	0.46	0.005	0.060	0.079	13.94	3705	8222
0.153	2.65	0.59	0.025	0.180	0.137	7.35	2277	2663
0.145	2.65	0.56	0.035	0.253	0.138	5.66	2674	2409
0.152	2.65	0.58	0.031	0.204	0.154	4.91	3264	2553
0.147	2.65	0.56	0.007	0.078	0.095	10.62	3319	5610
0.157	2.65	0.59	0.008	0.099	0.077	9.07	3533	5098
0.137	2.65	0.53	0.008	0.098	0.080	10.35	3438	5665
0.124	2.65	0.48	0.019	0.149	0.125	7.48	3325	3959
0.117	2.65	0.45	0.018	0.129	0.143	11.90	2976	5639
0.120	2.65	0.47	0.052	0.314	0.167	6.91	2204	2425
0.117	2.65	0.45	0.122	0.790	0.154	3.50	2307	1285
0.118	2.65	0.46	0.010	0.107	0.091	10.46	3186	5303
0.124	2.65	0.48	0.028	0.278	0.100	4.76	3505	2656
0.129	2.65	0.50	0.047	0.304	0.155	4.00	3543	2256
0.126	2.65	0.49	0.017	0.173	0.100	6.07	3621	3500
0.118	2.65	0.46	0.017	0.190	0.087	5.58	3519	3124
0.114	2.65	0.45	0.008	0.095	0.080	10.64	4146	7021
0.117	2.65	0.46	0.008	0.093	0.087	8.40	4836	6468
0.135	2.65	0.52	0.147	1.198	0.123	2.61	2771	1150
0.127	2.65	0.49	0.126	0.974	0.129	2.69	1785	764
0.127	2.65	0.49	0.126	0.974	0.129	2.69	1785	764
0.115	2.65	0.45	0.157	1.217	0.129	2.83	3002	1350
0.106	2.65	0.41	0.121	0.943	0.128	2.94	2541	1190
0.107	2.65	0.42	0.079	0.432	0.182	5.86	2334	2176
0.102	2.65	0.40	0.008	0.126	0.064	9.00	4144	5935
0.102	2.65	0.40	0.018	0.214	0.085	6.75	3387	3638
0.102	2.65	0.40	0.016	0.140	0.115	6.75	5180	5564
0.103	2.65	0.40	0.302	1.860	0.162	1.87	1983	589
0.109	2.65	0.42	0.058	0.377	0.154	3.63	5011	2893
0.106	2.65	0.41	0.027	0.157	0.173	5.89	5081	4759
0.106	2.65	0.41	0.045	0.440	0.102	5.15	3909	3203
0.109	2.65	0.42	0.079	0.537	0.146	2.90	4625	2136
0.113	2.65	0.44	0.052	0.398	0.132	3.56	4543	2576
0.110	2.65	0.43	0.192	1.152	0.167	1.44	3453	794
0.556	2.65	1.28	0.068	0.423	0.160	9.96	1536	2434
0.484	2.65	1.21	0.087	0.515	0.169	8.26	1646	2165
0.637	2.65	1.36	0.095	0.533	0.179	6.60	2392	2513
0.276	2.65	0.90	0.075	0.598	0.125	5.93	2350	2216

Table 6 (Concluded). Dune Geometry -- Douglas L. Inman (7)

D_g (mm)	s	N_{sc}	η/a	λ/a	η/λ	N_{sm}	$T\sqrt{\frac{(s-1)g}{D_g}}$	a/D_g
0.325	2.65	0.99	0.192	1.325	0.145	2.94	2299	1076
0.457	2.65	1.17	0.291	1.830	0.159	2.83	1882	849
0.415	2.65	1.12	0.242	1.602	0.151	2.60	2568	1064
0.432	2.65	1.14	0.239	1.553	0.154	3.28	2323	1213
0.441	2.65	1.16	0.296	1.714	0.173	3.07	2108	1029
0.441	2.65	1.16	0.282	1.774	0.159	3.07	2108	1029
0.514	2.65	1.24	0.337	1.982	0.170	2.34	2130	793
0.398	2.65	1.10	0.243	1.610	0.151	3.80	1614	975
0.359	2.65	1.05	0.286	1.856	0.154	3.20	2336	1189
0.470	2.65	1.19	0.346	2.159	0.160	3.14	1801	901
0.525	2.65	1.25	0.488	3.050	0.160	1.98	1809	571
0.432	2.65	1.14	0.343	2.223	0.154	2.37	2130	803
0.448	2.65	1.16	0.288	1.780	0.162	2.86	2281	1040
0.913	2.65	1.52	0.242	1.283	0.188	3.26	1731	898
0.460	2.65	1.18	0.157	0.942	0.167	4.24	1876	1265
0.457	2.65	1.17	0.131	0.916	0.143	4.25	1882	1274
0.195	2.65	0.71	0.449	3.139	0.143	2.17	202	70
0.123	2.65	0.48	0.561	3.367	0.167	2.73	254	110
0.344	2.65	1.02	0.525	3.176	0.165	5.31	759	642
0.595	2.65	1.32	0.239	1.571	0.152	3.73	577	342
0.221	2.65	0.78	0.233	1.397	0.167	3.57	574	326

APPENDIX C

VELOCITY DISTRIBUTION ALONG THE UPSTREAM FACE OF A DUNE

The fluid-velocity distribution along the streamline just above the upstream face of a two-dimensional dune is approximated by utilizing a potential-flow solution for the fluid motion above the duned bed. The potential-flow solution is obtained by means of an electric analogy for flow over a stationary boundary. In other words, the bounding streamline geometry, defined by the upstream face of the dune and the line of separation from the crest, is assumed to be stationary during a half cycle of the oscillatory fluid motion. Even though the fluid motion is unsteady during a half cycle, the flow net of velocity-potential lines and streamlines will remain constant by virtue of the assumption of a stationary bounding streamline just above the dune face.

The geometry of the lower bounding streamline is established by the shape of the upstream face of the dune and the line of separation from the crest. A circular arc is used to approximate experimental measurements (Figure 3) of the shape of a two-dimensional dune. In particular, the ratio of the dune height to dune wave length is 0.18. Qualitative observations (Figure 4) of the line of separation show that separation occurs at the crest and reattachment occurs in the trough. The assumed line of separation shown in Figure 5(a) is a circular arc which is tangent to the upstream face at the crest and reattaches at the center

of the trough.

The construction and dimensions of the electric analogy are illustrated in the sketch below. The bounding streamlines are boundaries (as A and B in the sketch) of dry-conductor paper. A constant electrical potential is maintained between electrodes C and D. Six dunes were included in the boundary, B, in order

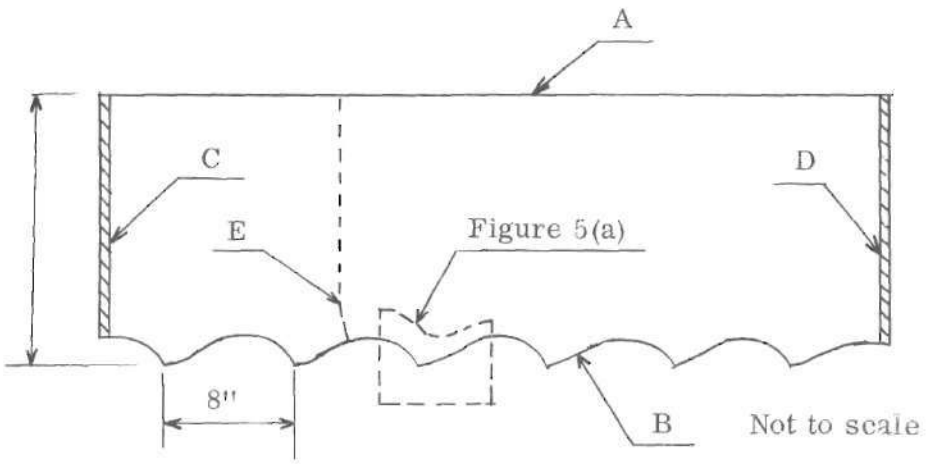

Sketch. Electric Analogy

to reduce the effect of the straight boundaries, C and D, in the control region. Lines of constant electrical potential, such as line E in the sketch, are determined by means of a probe and a voltage detector. The spacing of potential lines is chosen so that there is an equal voltage drop between successive potential lines. Streamlines are sketched normal to the potential lines. Only a small section, as shown in the sketch, of the complete flow pattern is reproduced in Figure 5(a).

The ratio of the spacing between two potential lines along the lower bounding streamline (just above the upstream face of the dune) to the spacing between the same two potential lines along the upper bounding streamline (in the mainstream flow) is

approximately equal to the velocity ratio, u/U. The value of u/U is at a point midway between the two potential lines along the lower bounding streamline. Values of u/U obtained from the flow net are shown in Figure 5(b) as open circles. Note that the solid line in Figure 5(b) is a linear approximation, equation 2, of the flow-net solution.

LITERATURE CITED

1. M. R. Carstens and Frank M. Neilson, "Evolution of a Duned Bed Under Oscillatory Flow," Journal of Geophysical Research, Vol. 72, No. 12, pp. 3053-3059.

2. R. A. Bagnold, "Motion of Waves in Shallow Water--Interaction Between Waves and Sand Bottoms," Proceedings of the Royal Society of London, Series A, Vol. 187, October 1946, pp. 1-18.

3. M. R. Carstens, F. M. Neilson, and H. D. Altinbilek, "An Analytical and Experimental Study of Bed Forms Under Water Waves," Project A-798, Engineering Experiment Station, Georgia Institute of Technology, Atlanta, Ga., September 1967.

4. John F. Kennedy and Marco Falcon, Wave-Generated Sediment Ripples, Report No. 86, Hydrodynamics Laboratory, Massachusetts Institute of Technology, Cambridge, Mass., August 1965.

5. S. Yalin and R. C. H. Russell, "Similarity in Sediment Transport due to Waves," Proceedings of the Eighth Conference on Coastal Engineering, 1962, Mexico City, Mexico, pp. 151-167.

6. Douglas L. Inman and Anthony J. Bowen, "Flume Experiments on Sand Transport by Waves and Currents," Proceedings of the Eighth Conference on Coastal Engineering, 1962, Mexico City, Mexico, pp. 137-150.

7. Douglas L. Inman, Wind-Generated Ripples in Nearshore Sands, Technical Memorandum No. 100, Beach Erosion Board, Department of the Army, Corps of Engineers, October 1957.

8. Madhav Manohar, Mechanics of Bottom Sediment Movement due to Wave Action, Technical Memorandum No. 75, Beach Erosion Board, Department of the Army, Corps of Engineers, June 1965.

9. Vincent and Ruellan, "Contribution to the Study of Sediment Transport on a Horizontal Bed Due to Wave Action," Proceedings of the Sixth Conference on Coastal Engineering, 1958.

10. A. R. Lefeuvre, Sediment Transport Functions with Special Emphasis on Localized Scour Unpublished Ph.D. Dissertation, Georgia Institute of Technology, May 1965.

11. B. O. Pierce, and Ronald M. Foster, A Short Table of Integrals, 4th Edition, Ginn and Company, N.Y., 1957.

VITA

Frank Murray Neilson was born in Edmonton, Alberta, Canada, on December 26, 1938. He attended local schools and, in 1957, graduated from Beaupre' High School, Onoway, Alberta, Canada. He entered the University of Alberta, Edmonton, in September 1957 and graduated, with a Bachelor of Science Degree in Civil Engineering, in May 1961. From May 1961 until September 1963 he was employed by the Canadian Hydrographic Service in Victoria, British Columbia, Canada. During these years he participated in surveys along the Western Coast of Canada, on the Kootenay Lake, and on the St. Lawrance River. In September 1963 he enrolled in graduate school at Georgia Institute of Technology and obtained the Master of Science Degree in Civil Engineering in June 1964. During the summer of 1964 he was employed by the Tesco Chemical Company of Atlanta, Georgia. He re-entered Georgia Institute of Technology, in pursuit of a Doctor of Philosophy degree, in September 1964.

During the period 1964-1968 he was employed as a Research Assistant and as such, participated in three projects of the Engineering Experiment Station of the Georgia Institute of Technology. During this period, he also was employed by the Civil Engineering Department as a Teaching Assistant and as a Research Hydraulic Engineer. Currently, from July 1968, he is employed as a Research Engineer with the Waterways Experiment Station, Corps of Engineers, Vicksburg, Mississippi.

He is a member of Sigma Xi and Chi Epsilon.

He is single.